January 2015

The role of snow in soil thermal dynamics of the arctic terrestrial ecosystems

Zhou Lyu
Purdue University

Graduate School Form 30
Updated 1/15/2015

PURDUE UNIVERSITY
GRADUATE SCHOOL
Thesis/Dissertation Acceptance

This is to certify that the thesis/dissertation prepared

By Zhou Lyu

Entitled

THE ROLE OF SNOW IN SOIL THERMAL DYNAMICS OF THE ARCTIC TERRESTRIAL ECOSYSTEMS

For the degree of Master of Science

Is approved by the final examining committee:

Greg Michalski
Chair

Laura C Bowling

Qianlai Zhuang

Melba M Crawford

To the best of my knowledge and as understood by the student in the Thesis/Dissertation Agreement, Publication Delay, and Certification Disclaimer (Graduate School Form 32), this thesis/dissertation adheres to the provisions of Purdue University's "Policy of Integrity in Research" and the use of copyright material.

Approved by Major Professor(s): Qianlai Zhuang, Melba M Crawford

Approved by: Indrajeet Chaubey 12/3/2015

Head of the Departmental Graduate Program Date

THE ROLE OF SNOW IN SOIL THERMAL DYNAMICS OF THE ARCTIC TERRESTRIAL ECOSYSTEMS

A Thesis

Submitted to the Faculty

of

Purdue University

by

Zhou Lyu

In Partial Fulfillment of the

Requirements for the Degree

of

Master of Science

December 2015

Purdue University

West Lafayette, Indiana

To my dearest parents.

ACKNOWLEDGEMENTS

There are many people that I would like to express my sincere gratitude to along the path of finishing this thesis study. I would like to start by thanking Dr. Qianlai Zhuang for his guidance, assistance, and encouragement. I started off with a different background and had very limited knowledge about the project, yet Dr. Zhuang has been inspiring and optimistic, in lightening up the path forward. It's been a great honor studying from and working under him. My gratitude also goes to Dr. Melba Crawford. She is an amazingly energetic person with a sharp mind. I just wish I could be like her at her age. She has always been supportive to me, and introducing me to various remote sensing data sources that might be helpful in my study with great enthusiasm. I would like to thank as well my other committee members: Dr. Laura Bowling, and Dr. Greg Michalski. Dr. Bowling is such a careful and amiable person with great knowledge on the topic of hydrology and snow dynamics, and has been a perfect supplement to my background. Even though I haven't started research relate to snow photolysis chemistry that is more of Dr. Michalski's interest, he has followed my research progress seriously, and provided many insightful suggestions along the study.

Special thanks to the data manager working at NOAA and NSIDC, for timely and detailed information on their data product that has been of great help for my research progress.

Finally I would like to thank the colleagues from the EBDL Lab and those who already moved on. I really appreciate the chance of working in the same lab with these smart and interesting future scholars and researchers. Thanks for the discussions and assistance that have been really helpful for my progress, and for making me feel surrounded.

It’s been two great years here at Purdue for me, and I’m looking forward to what Purdue will have for me in the years to come.

TABLE OF CONTENTS

Page

Page

LIST OF TABLES

Table Page

LIST OF FIGURES

Figure Page

Figure Page

Figure Page

Figure Page

Figure Page

Figure Page

Figure Page

Figure Page

Figure Page

Figure Page

ABSTRACT

Lyu,Zhou. M.S., Purdue University, December 2015. The role of snow in soil thermal dynamics of the arctic terrestrial ecosystems. Major Professor: Qianlai Zhuang. Co-advisor: Melba M. Crawford.

The vast area of permanent or seasonal snow cover is an essential component of terrestrial ecosystems in northern mid-to-high latitudes (45-90°N), which has insulation effects on the soil layer beneath it. The affected soil thermal regimes will impact soil carbon dynamics. Recent observations indicate that there are substantial changes in both snow cover extent and duration due to climate change in the area. It is important to understand the insulation effect historically so as to better quantify its role in affecting ecosystem carbon dynamics under changing climate in the future. This study incorporates the snow insulation effect by introducing a snow model into an existing soil thermal model in a biogeochemistry modeling framework, the Terrestrial Ecosystem Model (TEM). The coupled model is used to evaluate the effects of snow dynamics on thermal regimes in the pan-Arctic for the period 2003-2010. Available satellite snow-cover data and site-level data are used to calibrate and evaluate the modeling system for the historical period. The study demonstrates that the revised model reproduces the top-soil layers' thermal regime and freeze/thaw status reasonably well for the region. The study finds that the insulation effect of snow can alter soil thermal regime. The soil temperature

estimations at 5cm and 20cm depths using the satellite snow data are in general 5℃ warmer in winters compared to those using the previous version of the model. There is a lag of soil cooling rate in early winter and a lag of soil warming rate in late spring. The study also finds that the insulation effect of snow can influence ground freeze/thaw status. The frozen line estimated by the revised model moves slightly southward in late spring and slightly northward in early winter. This study suggests that future analysis of soil thermal and carbon dynamics should take snow dynamics into account for the region.

CHAPTER 1. INTRODUCTION

Rapid changes in the pan-Arctic climate have been reported over the past decades (IPCC, 2014). The changes are especially noticeable in the northern high latitudes, with a generally decrease in snow cover and frozen season duration, continual reduction of arctic sea ice, massive glaciers, and permafrost (Lemke et al., 20007). Satellite data reveals a significant reduction in snow cover extent (7% and 11% less snow covered area in the Northern Hemisphere compared with pre-1970 records for March and April) as well as an accelerated trend rate in the past 40 years (Brown and Robinson, 2011). However, the change of snow pack depth in the pan-Arctic shows a spatial variation. While a reduced snow depth is recorded in western North America over the past decades (Dyer and Mote, 2006), there has been an increase in annual snow depth in eastern Siberia (Park et al., 2014). This dramatic difference in cryosphere from the past, has, not-too-surprisingly, triggered consequent changes of the Arctic ecosystem. Observations and studies have shown that changes in Arctic albedo due to snow coverage and earlier onset of snowmelt (Déry and Brown, 2007) have been contributing to the fact that the warming trend in the pan-Arctic is stronger than that of the global mean (Serreze and Francis, 2006). Based on global climate model simulations (McCarthy, 2001), this stronger warming trend is most likely to continue. In addition, CCSM3 (Community Climate System Model) has predicted a 10~40% increase in winter snow fall, and a shortened

snow-period (-14 ± 7 days in spring, vs. $+20 \pm 79$ days in fall) from the twentieth to twenty-first century (Lawrence and Slater, 2010).

Playing a buffer role between the warming atmosphere and the soil layers, changes in snow pack will alter soil thermal conditions and microclimate. Snow is an insulator compared with most other ground surface materials. It has low thermal conductivity that can limit and modify heat transfer with the overlying atmosphere and underlying lithosphere, which directly affects the soil thermal regimes underneath. That largely explains why the magnitude of underground temperature variations in high latitudes does not directly respond to surface air warming (Lawrence and Slater, 2010). A deepening snow pack promotes warming shallow ground temperature, by enhancing the insulation of soil layers from the atmosphere, whereas a lengthened snow season prevents soil warming in spring due to decreased energy absorption. Studies have indicated a positive correlation between the snow depth and the snow period length (Beniston, 1997; Lawrence and Slater, 2010). In general, while it can be certain that winter snow cover affects soil temperature, the net effect of changing trends in snow condition on a larger temporal and spatial scale can either amplify or mitigate warming soils. Changing soil temperature, especially in winters, affects both soil and plant carbon processes (Zhang et al., 2008).

The Northern Hemisphere has a large area of boreal forest and sub-Arctic peatland and tundra, which hold a vast plant and soil carbon. In a recent study, the soil carbon pool of northern permafrost alone is estimated to be 495.80 Pg for the upper 100 cm depth, and 1024 Pg to 300 cm depth (Tarnocai et al., 2009). Taking deeper soil carbon

into account, the total organic carbon pool in the region is believed to be approximately 1672 Pg, constituting of almost half of the global organic carbon belowground (Tarnocai et al., 2009). In other studies, carbon storage in northern hemisphere permafrost area has been estimated to have twice as much carbon as the global atmosphere (Yi et al., 2015), and dry mass carbon in the northern forest and peatland accounts for one third of the global soil carbon (Gorham, 1991). These large carbon pools are extremely vulnerable to changes of soil temperature through carbon mobilization and decomposition processes.

According to the IPCC report, climate-induced changes are expected to continue, altering snow cover, permafrost stability, plant growing season length, and plant productivity in boreal and arctic ecosystems (Edenhofer et al., 2014). Will the major carbon sink in the northern high latitudes gradually transition to a large carbon source under future climate scenarios, and thus ultimately change the regional and global climate? With satellite data showing a continual reduction of annual mean snow cover extent and duration in the northern region (Yi et al., 2015), understanding how the soil thermal regime is being influenced and how this influence will further affect the large carbon pool in the pan-Arctic is needed. The magnitude of soil thermal variation is not homogeneous in the region, soil warming ranging from 30% to over 90% of surface air warming is simulated for different geographical locations (Lawrence and Slater, 2010). Studies have highlighted the importance of changes in near-ground air temperature and snow cover on thermal regimes in comparison with other factors (Osterkamp and Romanovsky, 1999; Osterkamp, 2007; Stieglitz et al., 2003). For instance, modeling studies concerning the North Slope of Alaska permafrost over the period of 1983-1998 showed that increasing snow pack contributes to the rising underground temperature to a similar level of

magnitude as the higher near-surface air temperature (Stieglitz et al., 2003). A mean decadal trend of 6.6 ± 12.0 cm soil active layer across the pan-Arctic is deepening due to widespread warming and lengthening of the non-frozen season. Increased seasonal snow cover extent is shown to promote warmer deep soil (≥ 0.5m) and more active soil respiration, and mitigates shallow surface soil decomposition in colder regions, while rising air temperature dominantly affects the upper soil temperatures in the warm-season (Yi et al., 2015). In a Community Land Model simulation, more than 50% of total thermal regime variations can be attributed to snow variability for the latter half of the twentieth century (Lawrence and Slater, 2010). However, this snow insulation effect in the larger pan-Arctic region has not been well quantified with process-based ecosystem models using recent satellite-based snow data.

This study used a process-based ecosystem model that includes a soil thermal model with remotely-sensed snow data to quantify the pan-Arctic snow-soil thermal interactions. This analysis neglects the phase change within the snow layer as well as the freezing and thawing induced thermal properties' change of the snow pack. A simple one-dimensional heat transfer snow-soil temperature module was incorporated into an extant Soil Thermal Model (STM; Zhuang et al., 2001) within the Terrestrial Ecosystem Model (TEM). The coupled model was then used to investigate soil thermal variations over the period of 2003-2010, with climate-induced changing snow cover and freezing/thawing processes in the pan-Arctic. The model can be used for both diagnostic modeling of present conditions and prognostic modeling of the future (Vorosmarty and Schloss, 1993; Zhuang et al., 2001, 2002, 2003, 2004, 2005; Felzer et al., 2005; Euskirchen et al., 2006). STM model was developed based on the Goodrich model

(Goodrich, 1976) and uses a finite element approach to determine heat flow in soils (Zhuang et al., 2001, 2002, 2003, 2004). Recent ground based datasets of climate, soil, vegetation, and elevation data at 0.5° latitude by 0.5° longitude spatial resolution are used to drive both the previous and revised modeling systems. The remotely-sensed snow data from AMSR-E/Aqua Level III product were used as an additional input for the revised model, to assess the role of snow in affecting topsoil column thermal dynamics.

CHAPTER 2. METHODS

2.1 Model description

In this study, TEM was coupled with an improved STM by including the effects of snow dynamics. The snow-soil heat exchange was explicitly modeled. Snow depth was estimated from satellite snow water equivalent data, and snow density was calculated based on a snow-classification system of Sturm et al. (1995, 2010). The simulated temperature at the bottom of the snow pack is used for the upper boundary condition of the soil profile. This simulated soil temperature is used to drive TEM to estimate soil carbon and nitrogen dynamics. The detailed structure and data flow in the revised TEM-STM system are presented in Figure 2-1.

TEM uses geographically-referenced climate, soil texture, elevation and vegetation data to estimate monthly carbon (C) and nitrogen (N) pool sizes and fluxes for various terrestrial ecosystem types. The model was firstly developed by Raich et al. (1991) and McGuire et al. (1992) to investigate net primary production (NPP) patterns in South and North America. The model was also used to quantify global carbon and nitrogen responses to changing climate (e.g., McGuire et al., 1995, 1997; McGuire et al., 1995). The improvement to the TEM modeling framework from this study is to have an explicit snow representation in the continuum of snow and soil system. The description of the main model structure and governing equations has been extensively documented in

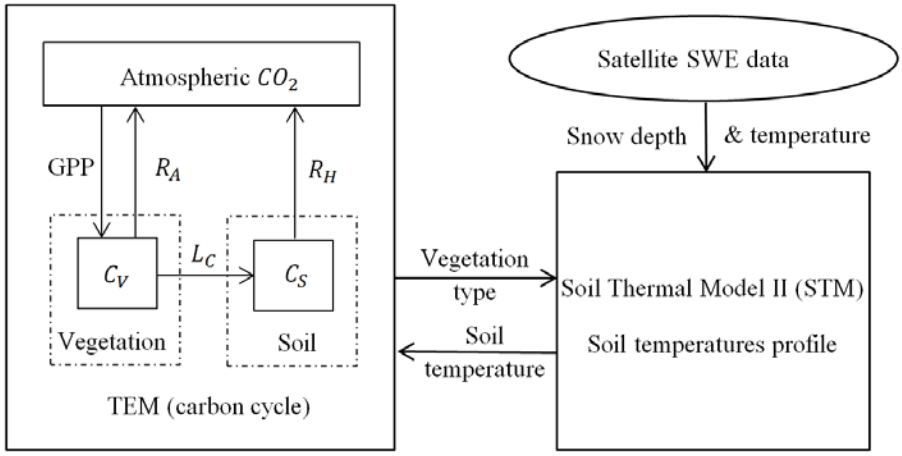

Figure 2-1. Flow of data in the coupled model, in which the soil thermal model (STM) receives snow depth information directly from the AMSR-E product and the revised STM feeds soil temperature profile to the terrestrial ecosystem model (TEM) for driving biogeochemical processes.

previous publications (Raich et al., 1991; McGuire et al., 1992, 1997; and Zhuang et al., 2003).

The extant Soil Thermal Model (STM) is a one-dimensional finite differential based model that was first developed to simulate soil thermal regime in Alaskan ecosystems with either a 0.5 hour or 0.5 day internal time step using either daily or monthly climate input data. The model was coupled into TEM for a number of applications at regional scales (Zhuang et al., 2001, 2002, 2003). STM models the heat fluxes within soils, with consideration of the phase change that accompanies freezing and thawing processes. The model estimates soil thermal dynamics at various soil layers including a snow layer, a moss layer, an upper organic layer, a lower organic layer, an upper mineral layer, and a lower mineral layer (Zhuang et al., 2001), as shown in Figure 2-2. Each layer is then further divided into finer sub-layers. In STM, every soil layer is prescribed a constant layer thickness, which is different for different vegetation types but is the same for grid cells in different geolocations of the same vegetation type. These layer thickness values were prescribed based on previous soil surveys, and have been inherited since the first coupled TEM-STM. Even though the individual vegetation type is assigned with different layer thickness for the same soil layer, the overall soil column thickness is the same for all vegetation types. Based on this layering system, the soil temperatures are estimated for each depth interval and time step for various soil layers.

The governing equation for heat conduction in soils and snow is:

$$F_z = -\lambda \nabla T \quad (1)$$

where F_z ($W \cdot m^{-2}$) is the amount of heat conducted across a unit cross-sectional area within unit time. λ ($W \cdot m^{-1} \cdot K^{-1}$) is the thermal conductivity of snow/soil, and ∇T ($K \cdot m^{-1}$) is the spatial gradient of temperature. The equation can be written in a one-dimensional form:

$$F_z = -\lambda \frac{\partial T}{\partial z} \tag{2}$$

where z (m) is in the vertical depth, both z and F_z are set to be positive upward.

To account for transient conditions, the continuous form of the energy conservation principle is invoked as:

$$c_g \frac{\partial T}{\partial t} = -\frac{\partial F_z}{\partial z} \tag{3}$$

where c_g ($J \cdot m^{-3} \cdot K^{-1}$) is the volumetric heat capacity of snow/soil, and t (s) is the time step.

Combining the previous two equations yields the second law of heat conduction in a one-dimensional form:

$$c_g \frac{\partial T}{\partial t} = \frac{\partial}{\partial z}\left(\lambda \frac{\partial T}{\partial z}\right) \tag{4}$$

The heat flux F_i from layer i to layer $i + 1$ at time step j is given by:

$$F_{i,j} = -k_{gi} \frac{T_{i,j} - T_{i+1,j}}{\Delta z} \tag{5}$$

where $T_{i,j}$ (K) is the snow/soil temperature at the i^{th} layer and the j^{th} time step. k_{gi} ($W \cdot m^{-1} \cdot K^{-1}$) is the snow/soil thermal conductivity and Δz is the layer depth.

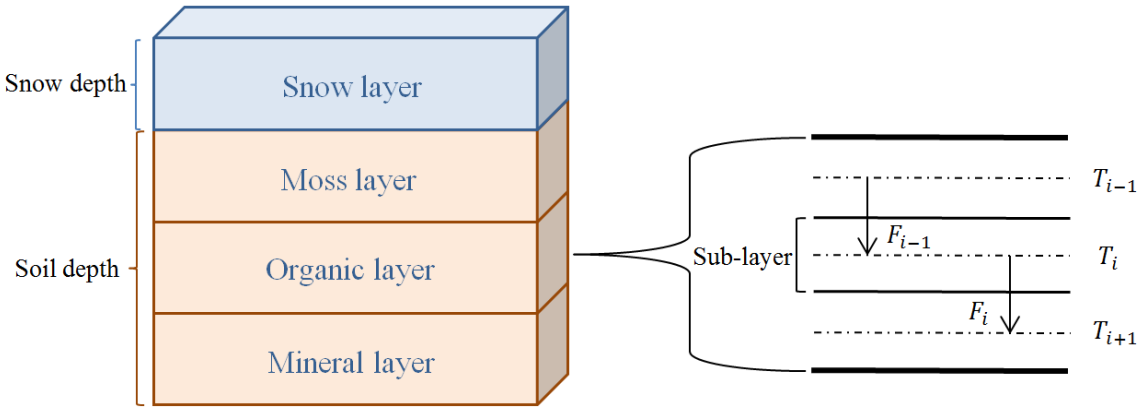

Figure 2-2. Schematic diagram of STM snow/soil column structure and sub-layers.

To drive the heat flux model, both upper boundary condition and lower boundary condition need to be specified. The upper boundary condition is defined to be the near-surface air temperature, and the lower boundary condition is assumed to be the heat flux out of the bottom of the snow/soil column, a constant value of $0.05\ \mathrm{W \cdot m^{-2}}$ (Osterkamp and Gosink, 1991; Zhuang et al., 2001).

The original STM model assumes a constant snow layer depth, snow cover extent and snow thermal property (Zhuang et al., 2001). Snow depth and extent were set to be constant across the space when air temperature is below 0℃. Meanwhile, snow thermal conductivities were different with respect to different vegetation types, and were prescribed based on the Sturm's snow classification system (Sturm et al., 1995). Other snow properties are the same among vegetation types. Such an approach can introduce discrepancies between observations and simulations when applied on a larger spatial scale. With more accurate, temporally and spatially available snow information from satellites, the constant snow insulation scheme was replaced in this study. The new snow module treats the snow pack explicitly in a snow-soil continuum. All model grids have snow depth information with different snow densities and thermal conductivities. The snow temperature at the bottom of the snow cover is used as the upper boundary condition for soil heat conduction equation. Previous research has indicated that the temperature profile within the snow pack generally follows a linear pattern, which is employed in this study (Cherkauer and Lettenmaier, 1999). The heat flux at the snow-soil interface from the snow side must be identical to the ground heat flux at the soil-snow interface coming from the soil column, calculated from the existing STM model. The upper boundary condition of the upper snow surface temperature is equal to the near-

ground air temperature, while the lower boundary condition at the snow-soil interface is allowed to change as equation (6):

$$K_{snow}\frac{\Delta T_{snow}}{\Delta Z_{snow}} = G = -K_{soil}\frac{\Delta T_{soil}}{\Delta Z_{soil}} \quad (6)$$

where K_{snow} is the snow thermal conductivity ($Wm^{-1}K^{-1}$), and K_{soil} is the soil thermal conductivity ($Wm^{-1}K^{-1}$). ΔZ_{snow} (m) is the snow depth, and ΔZ_{soil} (m) is the simulated soil column depth. ΔT_{snow} (℃) is the temperature change through the snow pack from snow surface (where the temperature is defined as air temperature) to snow base, and ΔT_{soil} (℃) in this particular module is the temperature change through the STM simulated soil column. Temperature at the bottom of snow is assumed to be the same as temperature at the soil surface, thus equation (6) can be expanded and written as:

$$T_{snowbase} = \frac{T_{air} + \frac{K_{soil}}{K_{snow}\cdot\Delta Z_{soil}}\cdot\Delta Z_{snow}\cdot T_{soilbase}}{1 + \frac{K_{soil}}{K_{snow}\cdot\Delta Z_{soil}}\cdot\Delta Z_{snow}} \quad (7)$$

The current month air temperature and calculated soil temperature profile from the previous time step are substituted into equation (7) to solve for the initial temperature at the bottom of snow. This initial temperature at the bottom of snow is then fed back to STM as the new upper boundary condition for an intermediate soil temperature profile from the explicit solution of equation (5), which is then substituted into equation (7) to solve for an intermediate temperature at the bottom of snow. These calculations are iterated for thirty times in order to balance the heat flux at the interface between snow and soil. The temperature at the bottom of snow from the last iteration is taken as the upper boundary condition to solve for the final soil temperature profile for the current

month. In contrast, the previous version of STM uses air temperature as the upper boundary condition.

The snow thermal conductivity used in equation (7) is approximated from its density, following the empirical relationship summarized by Sturm et al. (1997):

$$K_{snow} = 0.138 - \frac{1.01 \times \rho_{snow}}{1000} + 3.2\left(\frac{\rho_{snow}}{1000}\right)^2 \quad (8)$$

where ρ_{snow} ($kg \cdot m^{-3}$) is the density of the snow pack.

The soil thermal conductivity applied in the equation is the weighted average value of the values of the whole soil column, which are provided from precomputed parameter file that was calibrated for each ecosystem type for selected sites (see section 2.3).

The snow depth Z_{snow} in the heat flux equation is calculated from the snow water equivalent data, obtained from the satellite data product. Snow density bridges the snow depth and the snow water equivalent (SWE) with respect to the varying environment. Different types of snow cover have different snow densities, which are generally dependent on the types of the land surface and time since snow fall, as well as the properties of blowing wind (Sturm et al., 2001). With different densities of snow pack, snow depth can be varying even with the same SWE. Thus, a snow classification system for seasonal snow cover (Sturm et al., 1995) is implemented to dynamically estimate the snow depth. The equation for estimating snow depth from SWE is:

$$Z_{snow} = \frac{SWE \times \rho_{water}}{\rho_{snow}} \quad (9)$$

where SWE (m) is the observed snow water equivalent, defined as the amount of water contained in the snow pack; and ρ_{snow} ($kg \cdot m^{-3}$) is the snow density. The density used here is the bulk density that has considered both the density of fresh surface snow and compacted bottom snow, but does not reflect the densification process to allow the density vary with the season. Due to this simplification and the limitations of available data, density change since the snow fall due to compaction, precipitation, melting, refreezing, and wind-blowing is neglected here, although it is recognized that it impacts the accuracy of the snow depth calculation, and further the estimation of snow/soil temperature profile, especially for the transitional months in early winter and late spring. Similar to soil layer thickness, each vegetation type has a prescribed snow density as shown in Table 2-1. Here a minimum acceptable snow depth of 0.01 m is set, calculated snow depth shallower than this is ignored, considering the fact that shallow snow pack temperature basically equals the air temperature and has very limited insulation effects on the soil column.

Table 2-1. Snow density for different vegetation types

	Alpine tundra	**Wet tundra**	**Boreal forest**	**Coniferous forest**
Snow density ($\mathbf{kg \cdot m^{-3}}$)	312.0	360.0	214.0	214.0

2.2 Datasets

The modeling spatial domain for this study includes the whole pan-Arctic region (45°N above), encompassing Canada, Russia, Greenland, almost all of Europe and Mongolia, and the northern parts of China and the United States. The region includes multiple land surface and vegetation types (alpine tundra, wet tundra, boreal forest, and coniferous forest). The model was run at 0.5° by 0.5° spatial resolution under the UTM projection (Universal Transverse Mercator) and a monthly time step from 2003 to 2010. Detailed information on model calibration and driven datasets for this simulation are provided below.

2.2.1 Model inputs

The forcing data is divided into two main categories: 1) in situ data and re-analysis data include radiation, air temperature, precipitation, soil texture, elevation, and Leaf Area Index (LAI) and 2) the remotely-sensed satellite data of snow water equivalent. All data are organized for the area between 45°N and 90°N, and resampled or interpolated to the 0.5° latitude by 0.5° longitude spatial resolution.

Monthly climate data for the period of 2003 - 2010 include air temperature (℃), precipitation (mm), and radiation ($W \cdot m^{-2}$), which are obtained from the daily datasets of Climate Research Unit database (CRU, Mitchell et al., 2004). Specific, monthly air temperature and radiation are the monthly mean of the daily records, while monthly precipitation is the monthly accumulation of daily precipitation records. Annual mean air temperature and radiation, as well as annual accumulated precipitation, from 2003 to 2010 are shown in Figures 2-3 to 2-5. Aside from these time series data, the gridded

global-scale soil texture data is organized based on the Food and Agriculture Organization/United Nations Educational Scientific and Cultural Organization (FAO/UNESCO) [1974] soil map of the world. The input vegetation map is obtained from Melillo et al. (1993), and the elevation values for the whole study region are obtained from 10 min digital global elevation data (NCAR/Navy, 1984).

Global Monthly EASE-Grid Snow Water Equivalent data (SWE) is obtained from the National Snow & Ice Data Center (http://nsidc.org/data/docs/daac/ae_swe_ease-grids.gd.html). This data set comprises global, monthly satellite-derived snow water equivalent (SWE) from June 2002 through September 2011, including eight complete years (2003-2010). Annual accumulated snow water equivalent is shown in Figure 2-6. The global SWE is derived from the Advanced Microwave Scanning Radiometer – Earth Observing System (AMSR-E) instrument carried on the NASA Earth Observing System (EOS) Aqua satellite. The data set is further enhanced with MODIS land data to correct for forest attenuation. SWE values documented in this dataset are measured in the unit of mm, and range from 0 to 480 mm (previously set range). The recorded snow water equivalent in this region is generally within 500 mm, which coincides well with the satellite based values (Brown et al., 2003; Brown and Mote, 2009). The original spatial resolution and projection of the data is gridded as 25 km Equal-Area Scalable Earth Grids (EASE-Grids). In this study, SWE data from 2003 to 2010 for the interest region is re-projected to UTM and re-scaled to $0.5° \times 0.5°$ resolution.

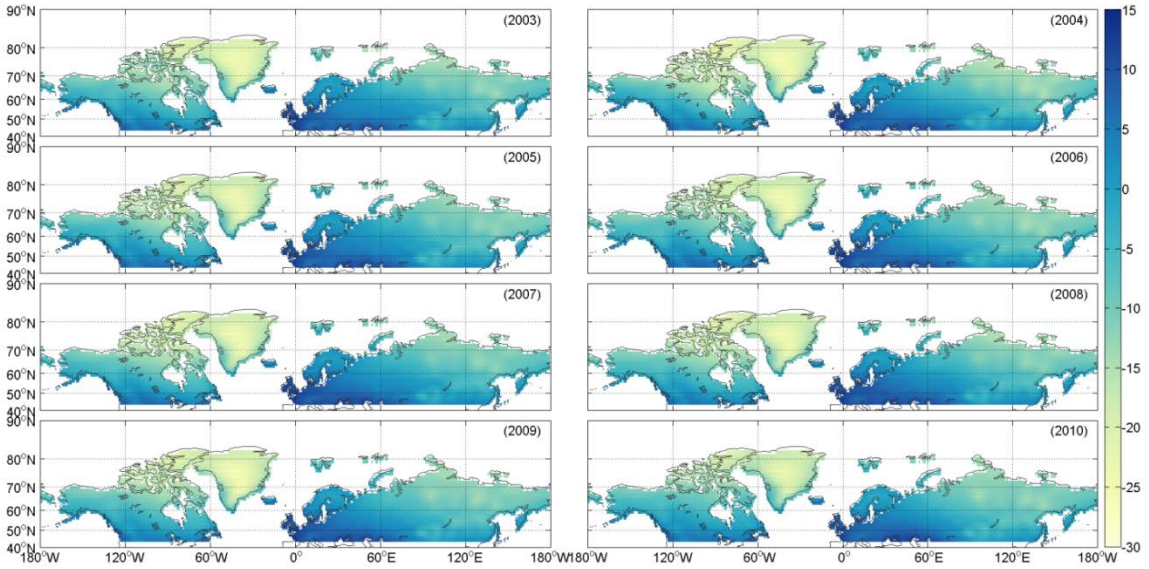

Figure 2-3. Annual mean air temperatures from 2003 to 2010 in the study region. The temperatures are displayed with units of ℃.

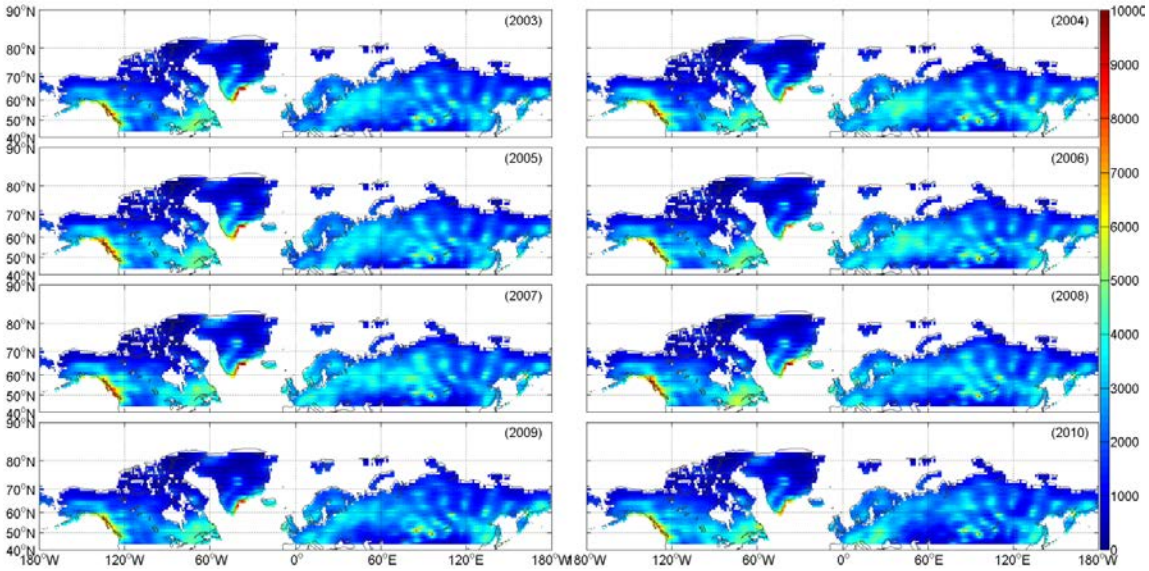

Figure 2-4. Annual accumulated precipitation from 2003 to 2010 in the study region. The precipitation is displayed with the units of mm.

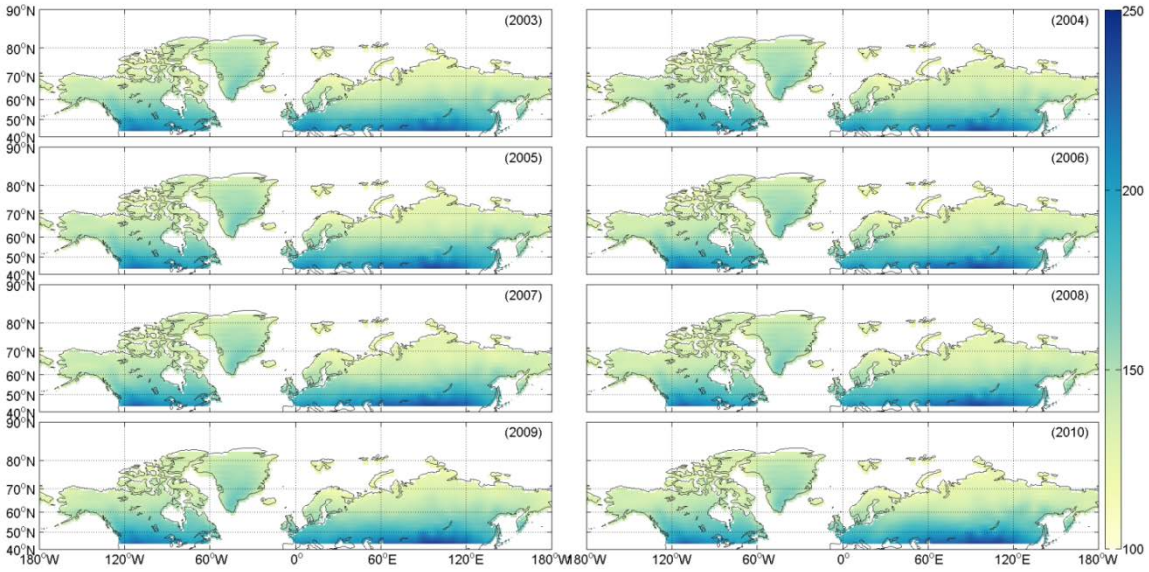

Figure 2-5. Annual mean incoming solar radiation from 2003 to 2010 in the study region. The radiation is displayed with the units of W/m^2.

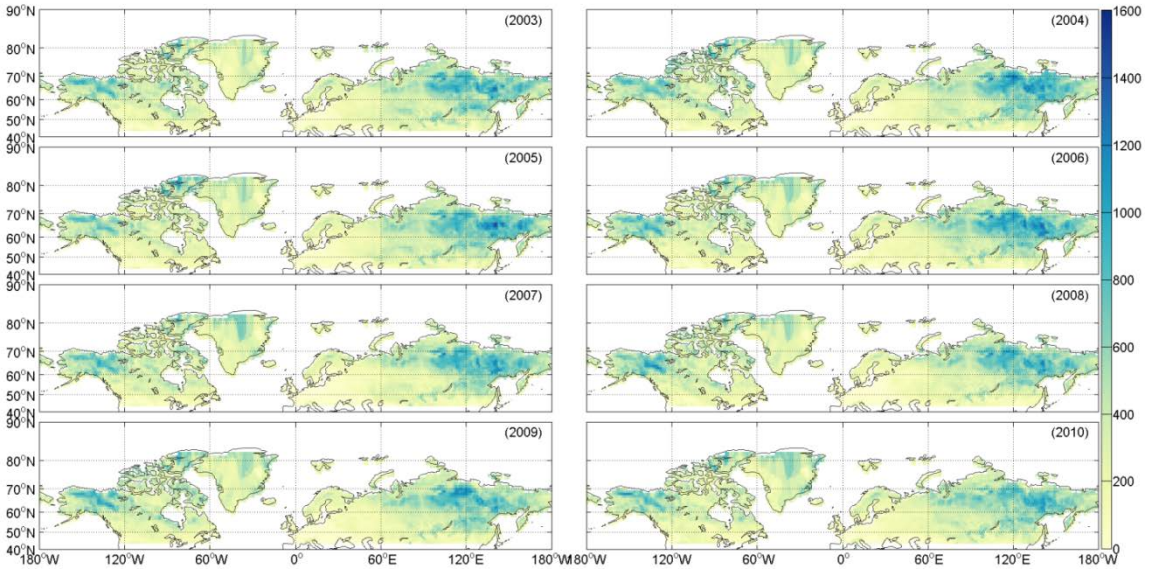

Figure 2-6. Annual accumulated snow water equivalent (SWE) from 2003 to in the study region. The SWE is displayed in the units of mm.

2.2.2 Parameterization data

To test the snow module performance and to calibrate parameters, several site-level simulations were conducted. Calibrations were performed separately for each of four major vegetation types in the region to obtain the optimal set of parameters. At each site, a set of climate and soil thermal data were obtained from the standardized Ameriflux Level II dataset at site-level (http://ameriflux.ornl.gov/). Major soil thermal and moisture parameters, such as soil heat capacity, soil heat conductivity and soil water content for the STM were calibrated so that the simulations match the observed underground soil temperatures.

Datasets used to the calibrate model include near ground air temperature, precipitation, and radiation as drivers and soil temperatures as evaluation data. Due to the harsh environmental condition and the limitation of measuring instrument in the Arctic, the observed datasets obtained are often intermittent or missing certain periods. This problem is especially evident for the alpine tundra research site in far northern Alaska with high latitudes and altitudes, where the equipment is removed during the long and cold polar season. Consequently, data is often collected only through March to October. Therefore the data sources are varying including one at a site in Alaska (Imnavait) to test for the alpine tundra ecosystem, one also from Alaska (Barrow) to test for wet tundra type land cover, one from Middle Canada (BOREAS NSA old black spruce forest) to test for boreal forest type, and finally two sites for coniferous forest type from the state of Maine (Howland Forest) and North Michigan (Sylvania Wilderness), respectively (Table 2-2). Simulations were driven mainly with these in-situ data, as well as high quality re-

analysis radiation data from NCEP as supplements. Standardized Ameriflux Level II climate and soil temperature measurements were taken at a half-hourly time step, which are then organized to monthly mean (such as air temperature) or monthly accumulation (such as precipitation) to work with monthly time step of TEM. Details on chosen sites for model calibration are documented below.

The Imnavait site (Imnavait Creek Watershed Tussock Tundra/US-ICt, 68.6°N, 149.3°W, from May 2008 to May 2010) is located near Imnavait Creek in Alaska, classified as an alpine tundra, with an average elevation of 930 meters. The site was established by the US Study of Environmental Arctic Change (SEARCH) program, as part of Arctic Observatory Networks (AON), in an effort to promote development of the pan-Arctic observing system that provides a full range of measurements of undergoing changes in the region. Currently, the project focuses on simultaneous measurements of carbon, water, and energy of the terrestrial landscape at an hourly time step. The tundra has precipitation throughout the year, with a long snow season starting from early September often until the beginning of June. Annual mean temperature is around $-7.4℃$ and maximum thawing depth of permafrost can be 25 to 100 cm depending on the specific environment. The site was equipped with a PAR Sensor measuring incoming radiation installed at a height of 3.2m above the surface of the basin, a 2.82m temperature and relative humidity probe to provide air temperature data, a surface rain gage for precipitation, and several thermocouple averaging soil temperature probes situated as deep as 0.08m for soil temperature recording (Ueyama et al., 2013).

The Barrow, Alaska site (Barrow/US-Brw, 71.3°N, 156.6°W, from January 2005 to December 2007) is a permanent wet tundra land cover, northeast to the northernmost city in the United States. The site is managed by the Biology Department of San Diego State University, aiming to record the carbon dioxide budget and its seasonal and inter-annual variation in the coastal Arctic region, and to quantify climate effects. The climate at Barrow is a typical polar climate, cold and dry with a long freezing season. Temperature probes, a tipping bucket rain gauge, a net radiometer, and thermocouples are installed in a similar fashion to the alpine tundra site (Ikawa and Oechel, 2014).

BOREAS NSA old black spruce forest (55.9°N, 98.5°W, from January 2003 to December 2006) is classified as a boreal forest, in south-central Canada near Thompson, Manitoba. Scientists from the Department of Soil Science of University of Manitoba have been working on the site during BOREAS (The Boreal Ecosystem-Atmosphere Study), a large scale climate-ecosystem interaction experiment beginning in the 1990s, to measure the carbon dioxide exchange and a full range of related climate factors. Mean annual air temperature of the region is $-3.2℃$, and mean annual precipitation is 51.7 cm (McCaughey et al., 1997; Amiro et al., 2006).

The Maine site (Howland Forest East Tower Harvest Site/US-Ho3, 45.2°N, 68.7°W, from January 2003 to December 2009) was chosen to be a parameterization site for the coniferous forest type. The Howland Forest research site is situated approximately 35 miles north of Bangor, within the Northern Experimental Forest of International Paper. This boreal-northern hardwood transitional forest consists of spruce-hemlock-fir, and hemlock-hardwood mixtures, and has a temperate continental climate. This site was

established by the University of Maine, with the cooperation of International Paper, and is currently been sponsored by the USDA Forest Service through its Global Change Program, the Department of Energy (DOE) through the NIGEC Program and the DOE Office of Science, and the National Science Foundation (NSF). The site provides air temperature, precipitation, and soil temperatures similar to the previous sites (Gaige et al., 2007). The only lacking observation is radiation, which is then provided by the gridded NCEP incoming radiation data.

The Sylvania Wilderness in North Michigan (Sylvania Wilderness/US-Syv, 46.2°N, 89.3°W, from January 2003 to December 2007) was used as a validation site for coniferous forest. The research site is a joint effort of University of Wisconsin, Ohio State University, and University of Minnesota, located in the Ottawa National Forest. The Sylvania Wilderness observation tower is one of the many towers operated under the Chequamegon Ecosystem Atmosphere Study (ChEAS), set up to understand the net ecosystem exchange of carbon in an undisturbed forest, and to compare the ecosystem's response to the climate variation of both the old-growth forest and the re-growing one. Similar to the previous coniferous forest site, the Sylvania Wilderness simulation also used NCEP radiation data because of the lack of in-situ measurements (Desai et al., 2005).

For all the soil thermal information obtained from Ameriflux Level II product, soil temperatures are recorded at one or two different soil depths in ℃ with measurement depth expressed in cm. Currently, measurement depths are limited within the near-surface underground soil layers; thus, the parameterization procedure was conducted focusing on the upper layers of the soil column. Specifically, measurement depths vary

with individual investigation site: 5 cm and 10 cm at both coniferous forest sites at Michigan and Maine, 10 cm at site BOREAS and Sylvania Wilderness, only 5 cm at site Barrow, and only at 2 cm at the alpine site of Imnavait.

Table 2-2. Site-level calibration data source

	Data link
Imnavait	http://ameriflux.ornl.gov/fullsiteinfo.php?sid=213
Barrow	http://ameriflux.ornl.gov/fullsiteinfo.php?sid=18
Boreas	http://ameriflux.ornl.gov/fullsiteinfo.php?sid=240
Sylvania	http://ameriflux.ornl.gov/fullsiteinfo.php?sid=58
Maine east	http://ameriflux.ornl.gov/fullsiteinfo.php?sid=53

2.2.3 Model evaluation data

Regional soil temperature simulations were evaluated using the North American Regional Reanalysis (NARR) soil temperature estimation provided by the NOAA/OAR/ESRL PSD, Boulder, Colorado, USA. This NARR data is a regional model reanalysis produced by the National Center for Environmental Prediction (NCEP) on the basis of large amounts of observational data (both field-based measurements and remotely sensed data) acquired across the entire continental North America. The NARR model then used these long-term observational data to assimilate the temperatures, winds, moistures, soil data, and other climate related properties. The soil temperature data, to be specific, is a regional model simulation using the coupled Noah LSM-Eta model, which focuses on estimating surface energy and water fluxes as well as the surface energy and water budgets in response to atmospheric forcing that has been assimilated into the model. The initial values of soil temperatures are all products of the coupled Noah LSM-Eta modeling system and land surface forcings that are internal to EDAS (the Eta Data Assimilation System) (Mesinger et al., 2006). The Noah LSM simulates soil temperature in four soil layers ranging $0-10$, $10-40$, $40-100$, and $100-200$ cm thickness (Ek et al., 2003). The dataset provides a full record covering the temporal period from 1979 to present day. The specific data used here is the NARR model simulated equal-distance-gridded (32.46341 km by 32.46341 km grid) monthly mean soil temperature averaging over the first 10 cm soil layer below ground produced by NARR-A model spanning 2003 to 2010 (http://nomads.ncdc.noaa.gov/data.php?name=access#narr_datasets). Because pixel to pixel comparison is not needed in this study, no resampling is preformed to this

dataset. Rather, the spatial average over the entire region is utilized in the evaluation that is discussed later.

Regional freeze/thaw status estimations were evaluated with the MEaSUREs Global Record of Daily Landscape Freeze/Thaw Status, Version 3 product. The original data set is a daily global record of the freeze/thaw (F/T) status of the earth surface processed from remotely-sensed radiometric brightness temperatures, provided by two satellite platforms. The first is from combining Scanning Multichannel Microwave Radiometer (SMMR, 1979-1986), Special Sensor Microwave/Imager (SSM/I, 1987-2008), and Special Sensor Microwave Imager/Sounder (SSMIS, 2009-2012) data at 37 GHz (vertical polarization) over the years 1979 to 2012. The second is from Advanced Microwave Scanning Radiometer-Earth Observing System (AMSR-E, 2002-2011) data at 36.5 GHz (vertical polarization) over the years 2002 to 2011. The specific microwave bands carried by the two platforms, which generate the brightness temperature record, can be used to identify soils as either frozen or non-frozen ground (Dugua and Pietroniro, 2005). The F/T status product is provided in the gridded format, with each grid cell projected to a global EASE-Grid format at a 25 km spatial resolution. The specific data set employed in this study is the Daily Composite (combined AM and PM) F/T status record derived from AMSR-E brightness temperature, for the eight complete years over 2003 - 2010. The original F/T status is displayed in four different categories: frozen (AM/PM frozen), thawed (AM/PM thawed), transitional (AM frozen and PM thawed), and inverse transitional (PM frozen and AM thawed). The latter two categories were merged into the frozen category in this study to simplify and to better compare with

model simulations. The data were processed to a monthly mean F/T status based on the mode status of each grid during the month.

2.3 Model parameterization and calibration

The revised STM was parameterized using the soil temperature simulation that matches the corresponding site measurement at various depths. Starting parameter ranges (Tables 2-3 to 2-6) were obtained based on previous sets of parameters from Zhuang et al. (2001). The optimization scheme used here is global optimization, aiming to find the set of parameters for each vegetation type that minimizes the discrepancy between observations and simulations. The estimates from TEM can be expressed as:

$$\widehat{Y} = f(X|\theta) + e \tag{10}$$

where $\widehat{Y} = (y_1, y_2, \cdots, y_n)$ is the model outputs vector containing time series of soil temperatures, f is the simplified expression of the simulation process functions built within the TEM model, X is the input data that drives the whole model, $\theta = (\theta_1, \theta_2, \cdots, \theta_m)$ is the vector of a set of m unknown parameters that are to be calibrated in this procedure. $e = [e(\theta_1), e(\theta_2), \cdots e(\theta_m)]$ are independently and identically distributed errors of the simulation (with zero mean and a constant variance).

Mathematically speaking, the goal of parameterization here is to generate thousands of parameter sets for the model, and through comparison between simulations and observations, to identify the set that minimizes the statistical error as defined previously. To assure the reliability of the parameterization and calibration results, the sample size shall be large enough to ensure parameter values are distributed within the parameter range. Here the sample size was set to be 10,000 different combinations of

parameters. The Latin hypercube sampling method was implemented to generate a samples based on a pre-defined parameters' value range (Iman, 2008). The parameterization procedure follows the steps below:

i) Initialize the parameter space. For each vegetation type, select parameters to be calibrated, and assign a specified range to each parameter $[(\theta_{1\_lower},\ \theta_{1\_upper}),\ (\theta_{2\_lower},\ \theta_{2\_upper}),\ \cdots,(\theta_{m\_lower},\ \theta_{m\_upper})]$ guided by previous studies (e.g., Zhuang et al., 2001) to start the sampling.

ii) Generate sample. Use Latin hypercube sampling method to generate testing sample. The Latin hypercube sampler randomly provides 10, 000 sets of parameters $(\theta_1, \theta_2, \cdots, \theta_m)$ from the starting range defined in (i).

iii) Run STM simulations at calibration sites. For each vegetation type, run the coupled STM for 10,000 times. Simulation results from all model runs are saved.

iv) Select optimal parameters. Sequentially compare all simulated soil temperatures with in-situ soil temperatures for each calibration type. Find the set that minimized the simulation error (minimized the RMSE).

Because of the limited in-situ data available for calibration, it was not possible to conduct both calibration and validation for each vegetation type with different site observations. Instead, each site was calibrated using at least three-years of data, and used remaining years' field-based data for model verification. The only exception, the coniferous forest type, is calibrated at Sylvania site, but validated at the Maine east site.

The starting ranges and optimized values of the calibrated parameters for all calibration and validation sites are shown in Tables 2-3 to 2-6. These parameters are vegetation type specific, and are used for each grid cell that is of the corresponding vegetation type: spatially different grid cells of the same vegetation uses the same set of calibrated parameters in the model run. Since these soil properties for each vegetation type were prescribed in the model run, the temporal change of these properties is neglected. This limitation is discussed later.

Table 2-3. Starting range and optimized parameter values calibrated in STM for tundra

Acronym	Definition	Starting	Optimized	Units
water1	Soil water content	[0.1, 0.8]	0.221	%
vcond1	Soil thermal conductivity	[0.01, 4]	0.561	$\mathrm{Wm^{-1}K^{-1}}$
vsph1	Soil heat capacity	[0.01, 4]	2.283	$\mathrm{MJm^{-3}K^{-1}}$
condt1	Thawing soil thermal conductivity	[0.01, 4]	0.023	$\mathrm{Wm^{-1}K^{-1}}$
spht1	Thawing soil heat capacity	[300, 3500]	2862.562	$\mathrm{KJm^{-3}K^{-1}}$
condf1	Frozen soil thermal conductivity	[0.01, 4]	1.261	$\mathrm{Wm^{-1}K^{-1}}$
sphf1	Frozen soil heat capacity	[300, 3500]	2782.689	$\mathrm{KJm^{-3}K^{-1}}$

Table 2-4. Starting range and optimized parameter values calibrated in STM for wet tundra

Acronym	Definition	Starting	Optimized	Unit
water1	Soil water content	[0.1, 0.8]	0.226	%
vcond1	Soil thermal conductivity	[0.01, 4]	3.331	$\mathrm{Wm^{-1}K^{-1}}$
vsph1	Soil heat capacity	[0.01, 4]	0.134	$\mathrm{MJm^{-3}K^{-1}}$
condt1	Thawing soil thermal conductivity	[0.01, 4]	2.97	$\mathrm{Wm^{-1}K^{-1}}$
spht1	Thawing soil heat capacity	[300, 3500]	349.28	$\mathrm{KJm^{-3}K^{-1}}$
condf1	Frozen soil thermal conductivity	[0.01, 4]	2.706	$\mathrm{Wm^{-1}K^{-1}}$
sphf1	Frozen soil heat capacity	[300, 3500]	1573.912	$\mathrm{KJm^{-3}K^{-1}}$

Table 2-5. Starting range and optimized parameter values calibrated in STM for boreal forest

Acronym	Definition	Starting	Optimized	Unit
water1	Soil water content	[0.1, 0.8]	0.18	%
vcond1	Soil thermal conductivity	[0.01, 4]	1.87	$Wm^{-1}K^{-1}$
vsph1	Soil heat capacity	[0.01, 4]	1.6	$MJm^{-3}K^{-1}$
condt1	Thawing soil thermal conductivity	[0.01, 4]	1.87	$Wm^{-1}K^{-1}$
spht1	Thawing soil heat capacity	[300, 3500]	1096.76	$KJm^{-3}K^{-1}$
condf1	Frozen soil thermal conductivity	[0.01, 4]	0.27	$Wm^{-1}K^{-1}$
sphf1	Frozen soil heat capacity	[300, 3500]	3389.64	$KJm^{-3}K^{-1}$

Table 2-6. Starting range and optimized parameter values calibrated in STM for coniferous forest

Acronym	Definition	Starting	Optimized	Unit
water1	Soil water content	[0.1, 0.8]	0.427	%
vcond1	Soil thermal conductivity	[0.01, 4]	0.98	$Wm^{-1}K^{-1}$
vsph1	Soil heat capacity	[0.01, 4]	1.066	$MJm^{-3}K^{-1}$
condt1	Thawing soil thermal conductivity	[0.01, 4]	1.836	$Wm^{-1}K^{-1}$
spht1	Thawing soil heat capacity	[300, 3500]	2313.505	$KJm^{-3}K^{-1}$
condf1	Frozen soil thermal conductivity	[0.01, 4]	0.029	$Wm^{-1}K^{-1}$
sphf1	Frozen soil heat capacity	[300, 3500]	2265.01	$KJm^{-3}K^{-1}$

2.4 Regional extrapolation

To examine how snow cover affects soil thermal regime in the mid-to-high northern latitudes, two sets of model simulations were conducted: (1) simulations with the previous TEM (TEM_S1 model), not considering the thermal effects of changing snow cover; and (2) simulations with the revised STM-TEM (TEM_S2 model) that has taken satellite-derived snow water equivalent data to drive the thermal dynamic module. The TEM_S1 simulations were driven with air temperature, precipitation, and radiation data from NCEP re-analysis data, and TEM_S2 simulations were driven with AMSR-E remotely sensed snow water equivalent data, in addition to the three climate forcing data mentioned above. These simulations were evaluated by comparing with the NARR model estimation of soil temperatures for both growing and non-growing season in North America.

CHAPTER 3. RESULTS AND DISCUSSION

3.1 Calibration results

The revised STM-TEM reproduced the ground-based estimate of soil temperatures at topsoil layers for alpine tundra, wet tundra, boreal forest and coniferous forest vegetation types with good fidelity(Table 3-1). The regression between the field measurement and revised model simulation exhibited a R^2 ranging from 0.81 to 0.98 for the four different calibrated vegetation types (Table 3-1 and Figures 3-1 to 3-6). Regression slopes are close to 1 for most sites, which show an excellent linearity, and the fitted intercepts are small. The root mean squared errors (RMSE) of all calibrated sites are listed in Table 3-1. The southern vegetation types generally behave better (1.45 ℃ RMSE for boreal forest site and $1.5 - 1.6$ ℃ RMSE for coniferous forest site) compared with those of the more northern types (2.20℃ RMSE for alpine tundra site and 2.81 ℃ RMSE for wet tundra site). Given the fact that site-level snow cover observation is not available, satellite snow water equivalent data were used as model input in the calibration process, which inevitably introduces a major uncertainty. The spatial resolution of the gridded satellite snow water equivalent data is very coarse for site-level simulation, considering the topography, vegetation cover and surface wind influence on the snow pack. For example, the Imnavait, the alpine tundra research site has a varied terrain. This topography diversity contributes to very different snow pack depths even within one site,

Table 3-1. Revised model site-level evaluation statistics for the four calibrated vegetation types

Site	Vegetation type	RMSE (℃)	R^2	Slope	Intercept
Imnavait	Alpine tundra	2.20	0.81	0.82	0.91
Barrow	Wet tundra	2.81	0.93	0.76	-1.61
Boreas	Boreal forest	1.46	0.86	0.84	0.65
Sylvania ts1	Coniferous forest	1.56	0.98	1.12	-1.58
Sylvania ts2	Coniferous forest	1.63	0.95	1.01	-0.50
Maine east	Coniferous forest	1.62	0.93	1.02	-0.43

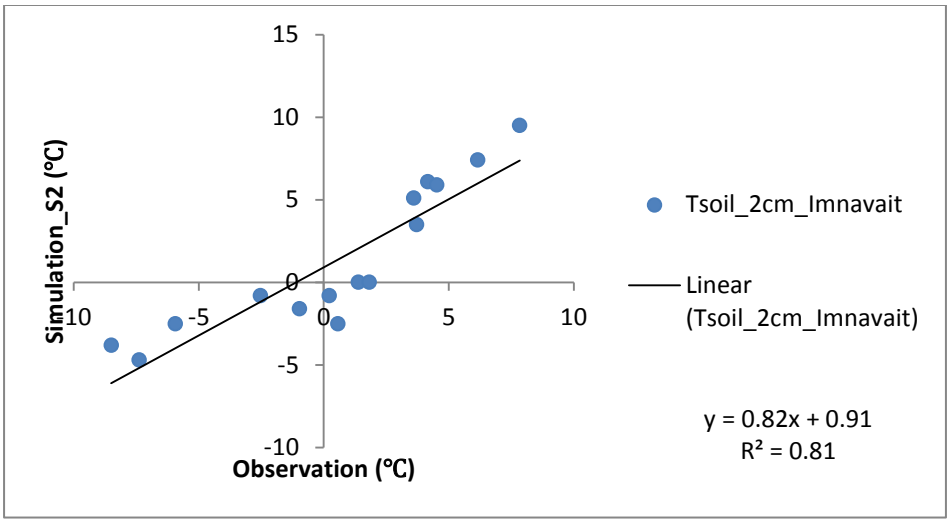

Figure 3-1. Calibration statistics and regression between revised model estimations (simulation_s2) and field measurements (observation) at the Imnavait research site (alpine tundra type), corresponding to soil temperature 2cm below ground during 2008-2010.

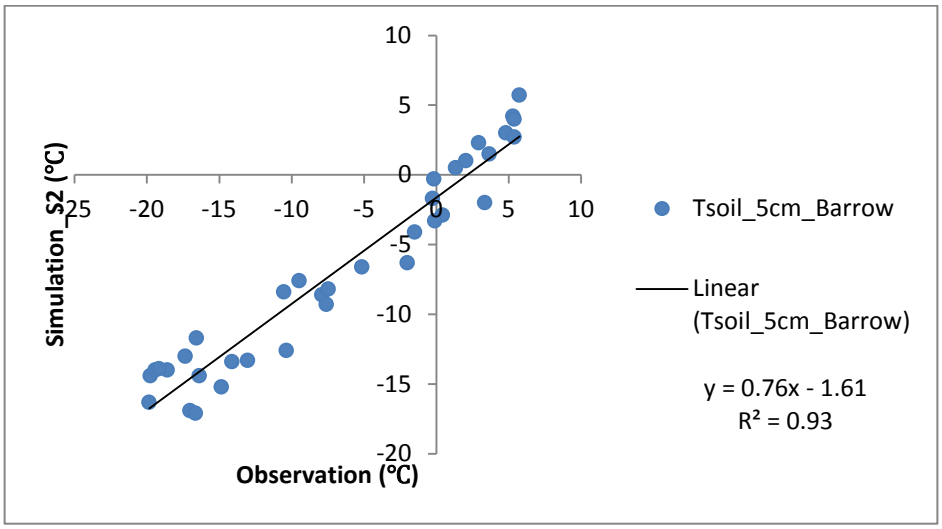

Figure 3-2. Calibration statistics and regression between revised model estimations (simulation_s2) and field measurements (observation) at the Barrow research site (wet tundra type), corresponding to soil temperature 5cm below ground during 2005-2007.

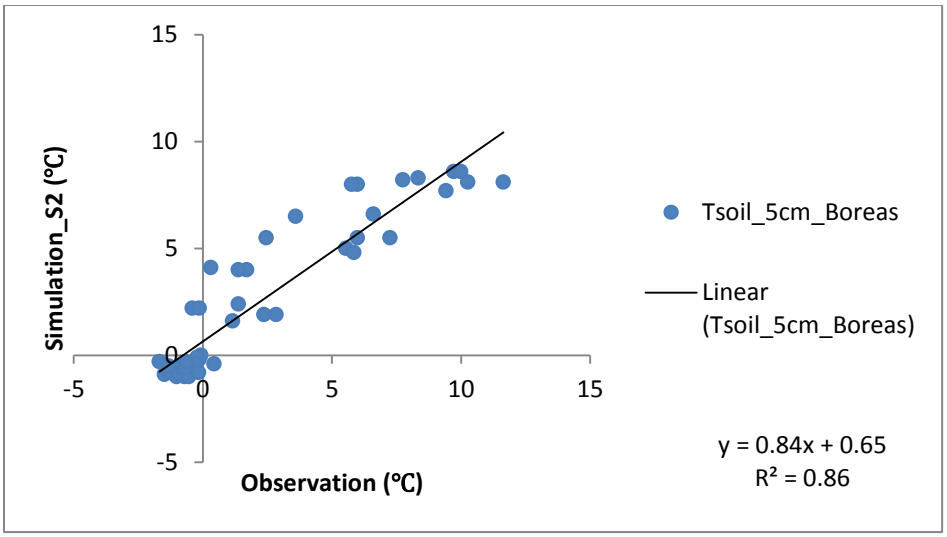

Figure 3-3. Calibration statistics and regression between revised model estimations (simulation_s2) and field measurements (observation) at the Boreas research site (boreal forest type), corresponding to soil temperature 5cm below ground during 2003-2006.

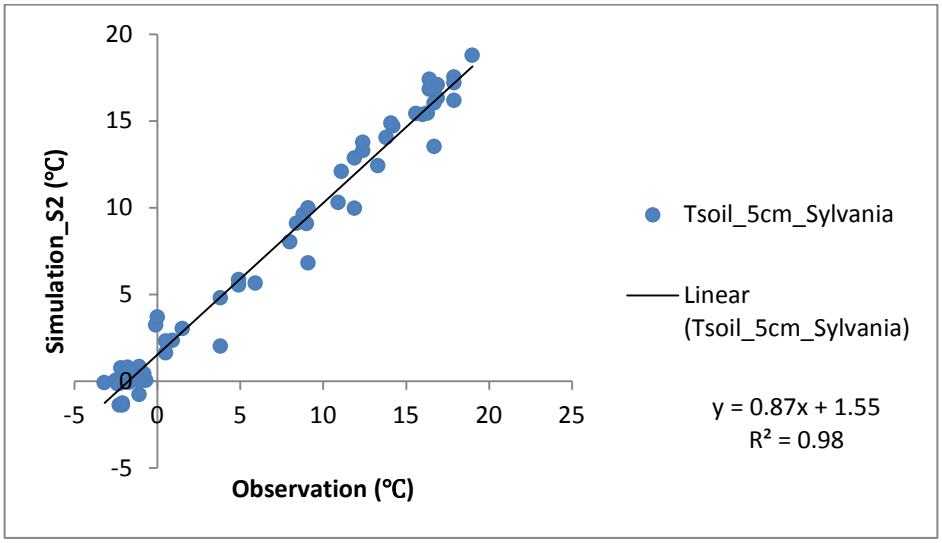

Figure 3-4. Calibration statistics and regression between revised model estimations (simulation_s2) and field measurements (observation) at the Sylvania research site (coniferous forest type), corresponding to soil temperature 5cm below ground during 2003-2007.

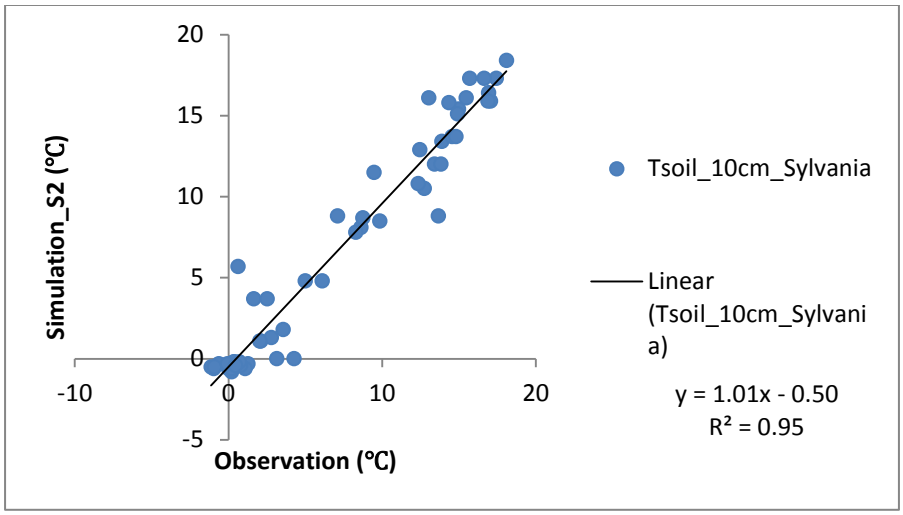

Figure 3-5. Calibration statistics and regression between revised model estimations (simulation_s2) and field measurements (observation) at the Sylvania research site (coniferous forest type), corresponding to soil temperature 10cm below ground during 2003-2007.

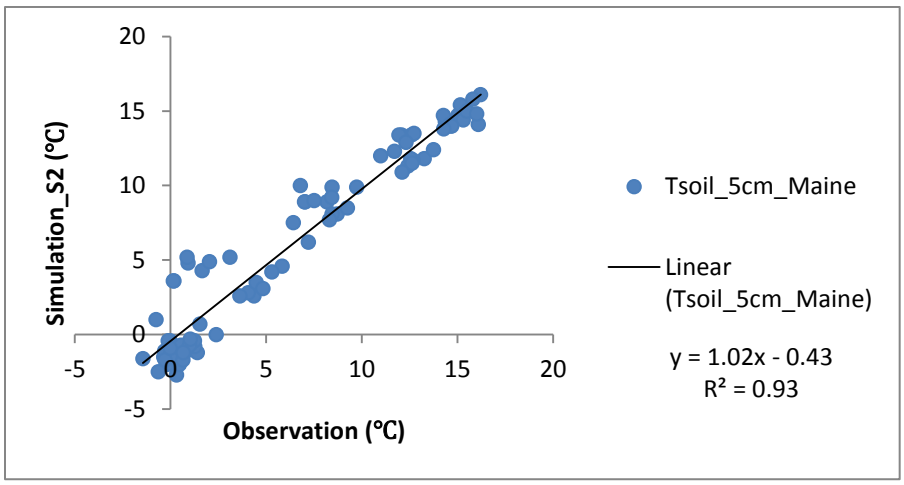

Figure 3-6. Calibration statistics and regression between revised model estimations (simulation_s2) and field measurements (observation) at the Maine east research site (coniferous forest type), corresponding to soil temperature 5cm below ground during 2003-2009.

which affects ground thermal characteristics, yet cannot be captured by the satellite snow observation data used in this study. The heterogeneity of these factors within one grid cell in the far north region can be substantial, leading more scattered simulation. However, overall, the revised STM-TEM model is able to better capture the observed soil temperature at various sites than the original model.

Site-level simulation comparisons between the two models demonstrate that the revised model is more capable of capturing the observed soil temperature profiles in the winter periods (Figures 3-7 to 3-12). Considering the insulation effect of snow cover on the soil column in the revised model significantly improves estimates of the soil temperature in the top. Using the temperature at the bottom of snow as the upper boundary conditions in the revised model reproduced field-based measurements well. The revised model estimates, that, in the snow season, several degrees centigrade higher (some times over $10℃$) in comparison with the previous model (Figures 3-7 to 3-12). Snow depth manipulation research has been conducted before in New Hampshire, in which treatment plots were kept snow free from the first autumn snowfall to early February to quantify the effects of decreased snow pack on soil freezing (Hardy et al., 2001). The research confirmed colder soil compared with the undisturbed reference plots with natural snow accumulation rates. Within top 10 cm soil layer, mean soil temperatures from the reference plots are approximately $3 - 5℃$ higher than those of the manipulated treatment plots. This suggests that there are prominent insulation effects of snow on soil thermal regimes, and that our model is able to capture the effects within reasonable magnitudes. This insulation effect is also evident in warm months, where the topsoil temperatures are usually a few degrees lower than the air temperatures.

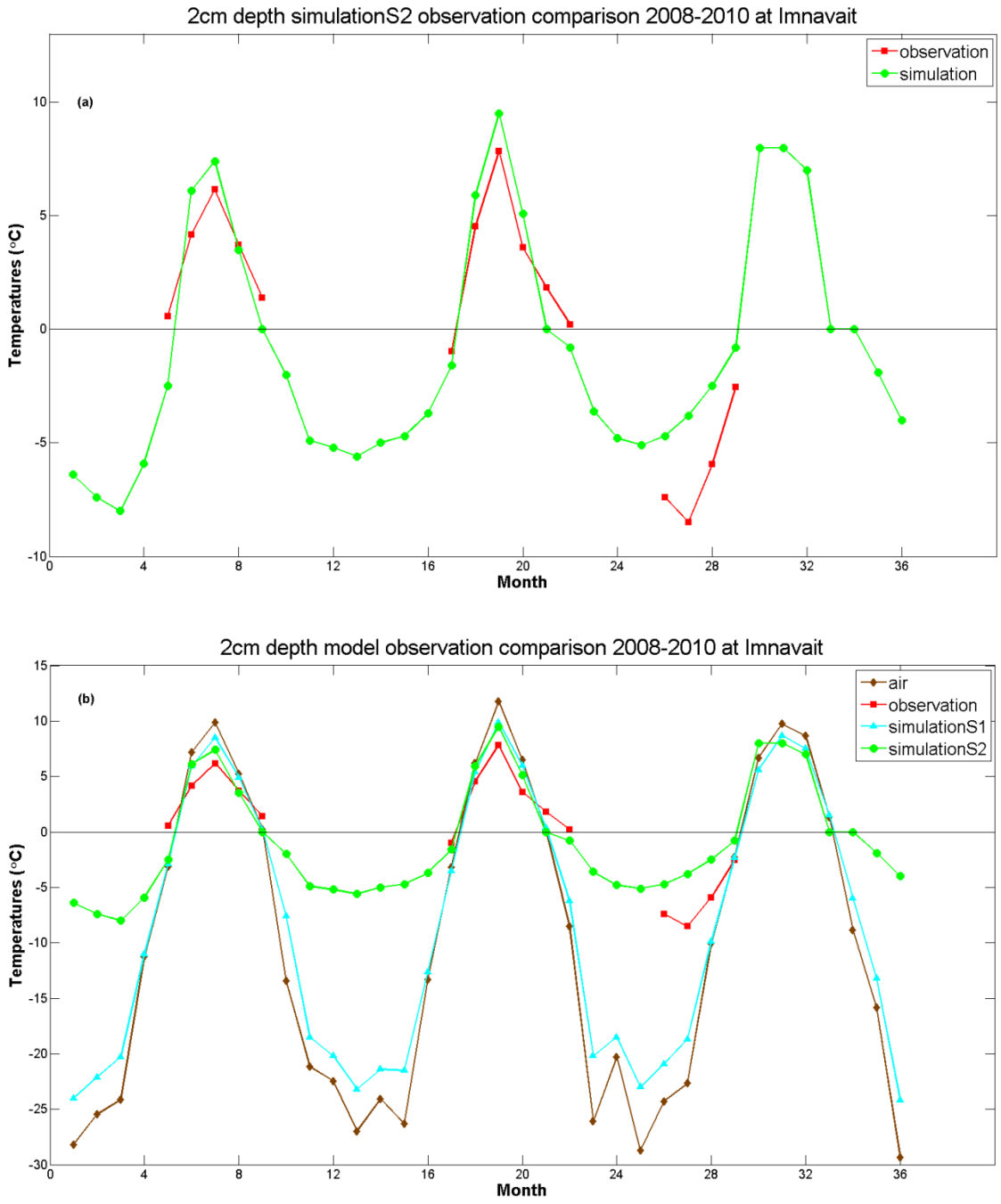

Figure 3-7. (a) Monthly averaged observed and revised simulated soil temperatures at 2 cm from 2008 to 2010 at the Imnavait research site (alpine tundra type). The red line and the squares represent the monthly averaged field-based measurements at 2 cm depth, while the green line and the dots represent the model simulations at the same depth from

revised model. (b) Monthly-averaged observations of both air temperature and soil temperature, simulations from the two versions of models at 2 cm depths from 2008 to 2010 at the Imnavait research site (alpine tundra type). The red line and the squares represent the monthly averaged field-based measurements at 2 cm depth, the yellow line and the diamonds represent the monthly mean air temperature, the blue line and the triangles represent the original model simulation at 2 cm depth, while the green line and the dots represent the model simulations at the same depth from revised model. The temperatures are displayed in the units of ℃.

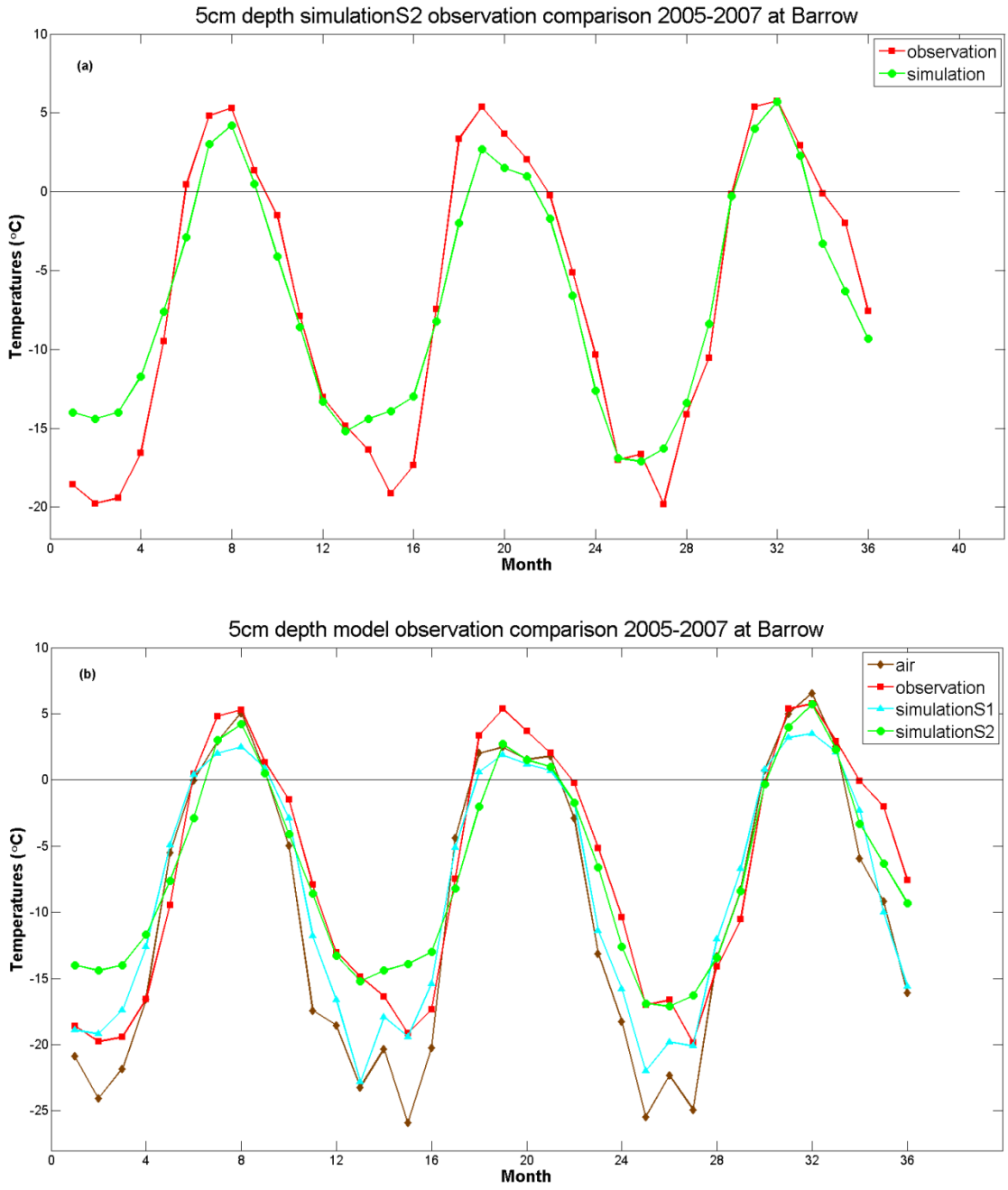

Figure 3-8. (a) Monthly averaged observed and revised simulated soil temperature at 5 cm depth from 2005 to 2007 at the Barrow research site (wet tundra type). The red line and the squares represent the monthly averaged field-based measurements at 5 cm depth, while the green line and the dots represent the model simulations at the same depth from

revised model. (b) Monthly averaged observations of both air temperature and soil temperature, simulations from the two versions of models at 5 cm depth from 2005 to 2007 at the Barrow research site (wet tundra type). The red line and the squares represent the monthly averaged field-based measurements at 5 cm depth, the yellow line and the diamonds represent the monthly mean air temperature, the blue line and the triangles represent the original model simulation at 5 cm depth, while the green line and the dots represent the model simulations at the same depth from revised model. The temperatures are displayed in the unit of ℃.

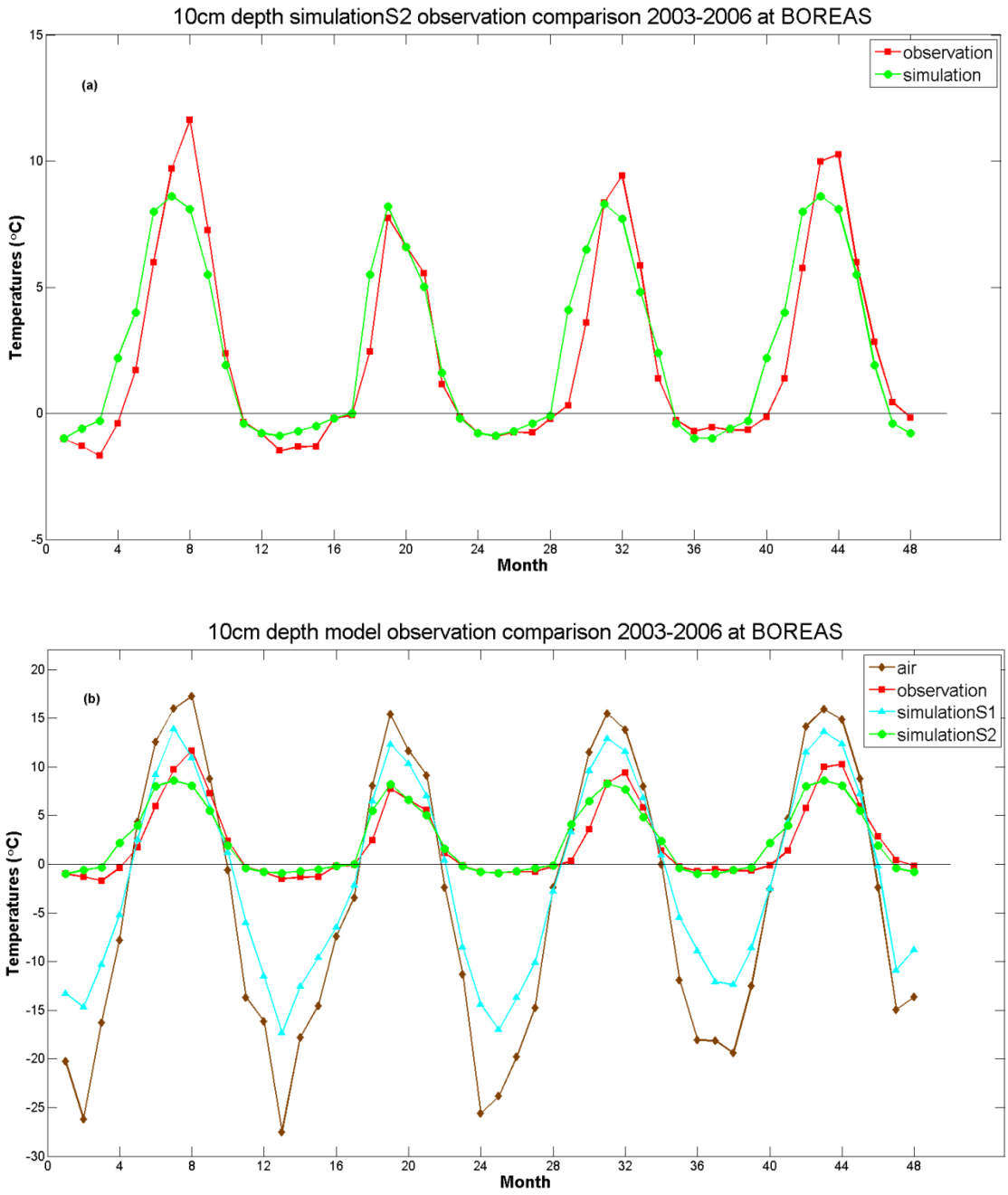

Figure 3-9. (a) Monthly averaged observed and revised simulated soil temperature at 10 cm depth from 2003 to 2006 at the Boreas research site (boreal forest). The red line and the squares represent the monthly averaged field-based measurements at 10 cm depth, while the green line and the dots represent the model simulations at the same depth from

revised model. (b) Monthly averaged observations of both air temperature and soil temperature, simulations from the two versions of models at 10 cm depth from 2003 to 2006 at the Boreas research site (boreal forest type). The red line and the squares represent the monthly averaged field-based measurements at 10cm depth, the yellow line and the diamonds represent the monthly mean air temperature, the blue line and the triangles represent the original model simulation at 10 cm depth, while the green line and the dots represent the model simulations at the same depth from revised model. The temperatures are displayed in the unit of ℃.

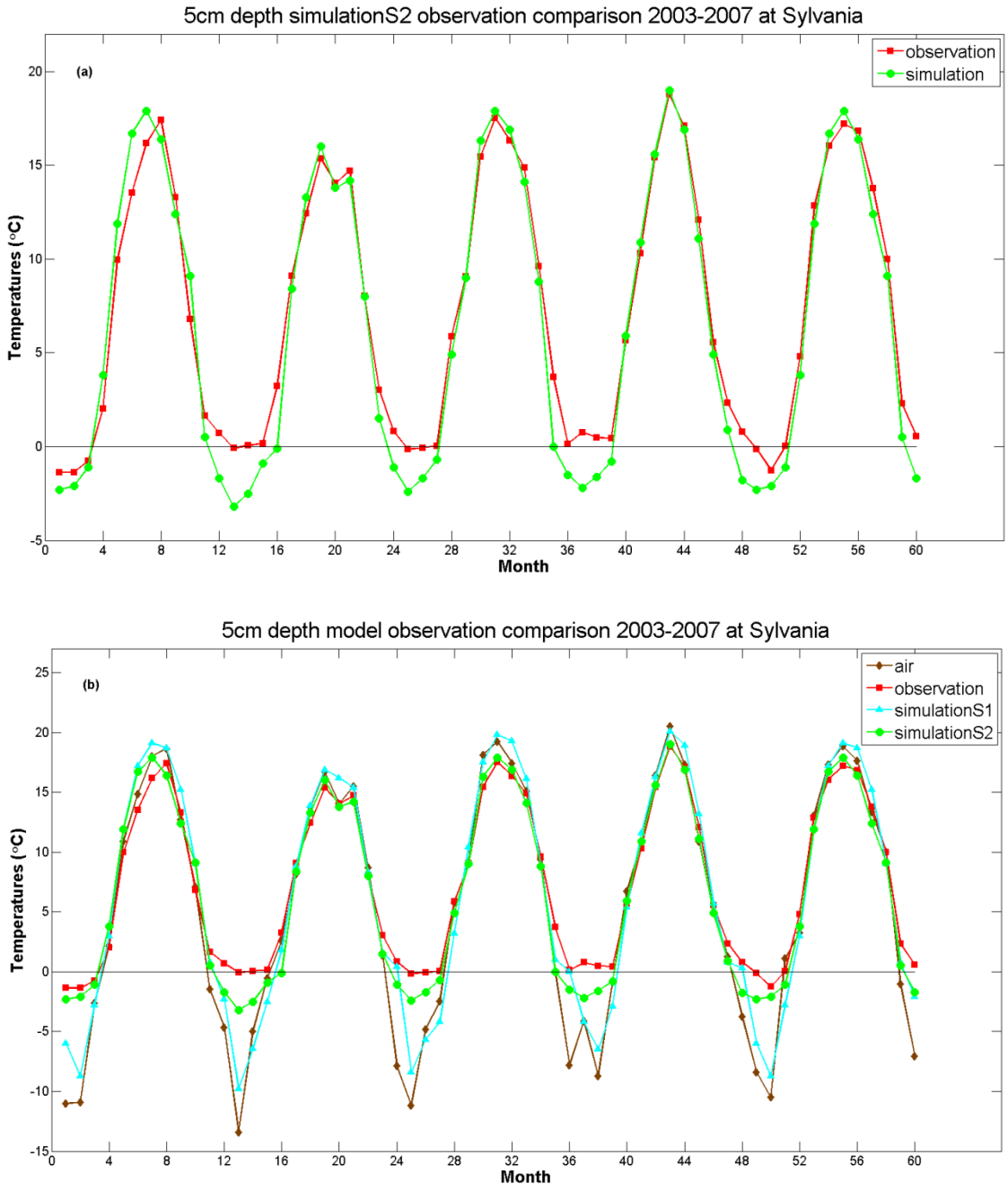

Figure 3-10. (a) Monthly averaged observed and revised simulated soil temperature at 5 cm depth from 2003 to 2007 at the Sylvania research site (coniferous forest type). The red line and the squares represent the monthly averaged field-based measurements at 5 cm depth, while the green line and the dots represent the model simulations at the same

depth from revised model. (b) Monthly averaged observations of both air temperature and soil temperature, simulations from the two versions of models at calibrated depth from 2003 to 2007 at the Sylvania research site (coniferous forest type). The red line and the squares represent the monthly averaged field-based measurements at 5 cm depth, the yellow line and the diamonds represent the monthly mean air temperature, the blue line and the triangles represent the original model simulation at 5 cm depth, while the green line and the dots represent the model simulations at the same depth from revised model. The temperatures are displayed in the unit of ℃.

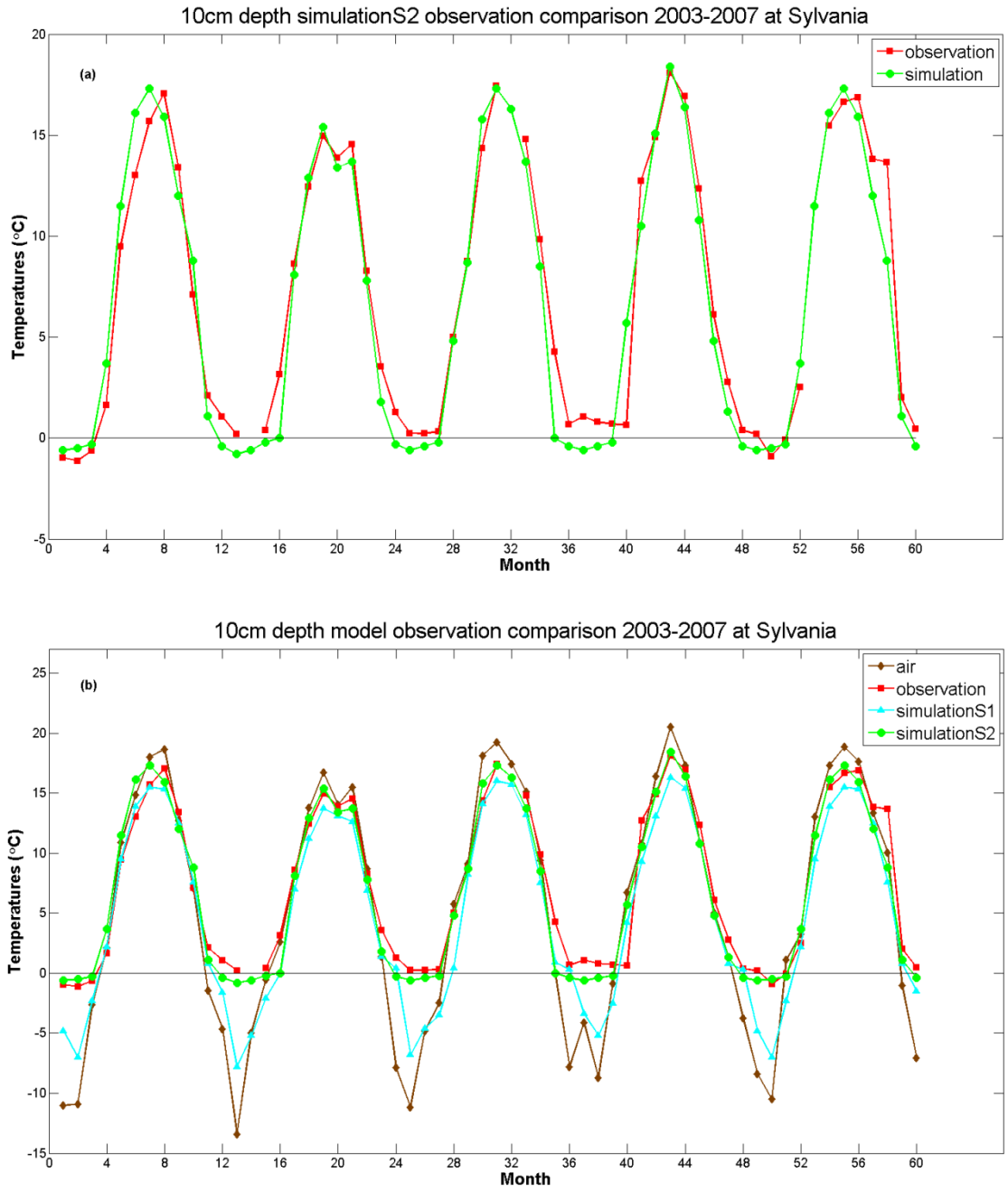

Figure 3-11. (a) Monthly averaged observed and revised simulated soil temperature at 10 cm depth from 2003 to 2007 at the Sylvania research site (coniferous forest type). The red line and the squares represent the monthly averaged field-based measurements at 10 cm depth, while the green line and the dots represent the model simulations at the

same depth from revised model. (b) Monthly averaged observations of both air temperature and soil temperature, simulations from the two versions of models at 10 cm depth from 2003 to 2007 at the Sylvania research site (coniferous forest type). The red line and the squares represent the monthly averaged field-based measurements at 10 cm depth, the yellow line and the diamonds represent the monthly mean air temperature, the blue line and the triangles represent the original model simulation at 10 cm depth, while the green line and the dots represent the model simulations at the same depth from revised model. The temperatures are displayed in the unit of ℃.

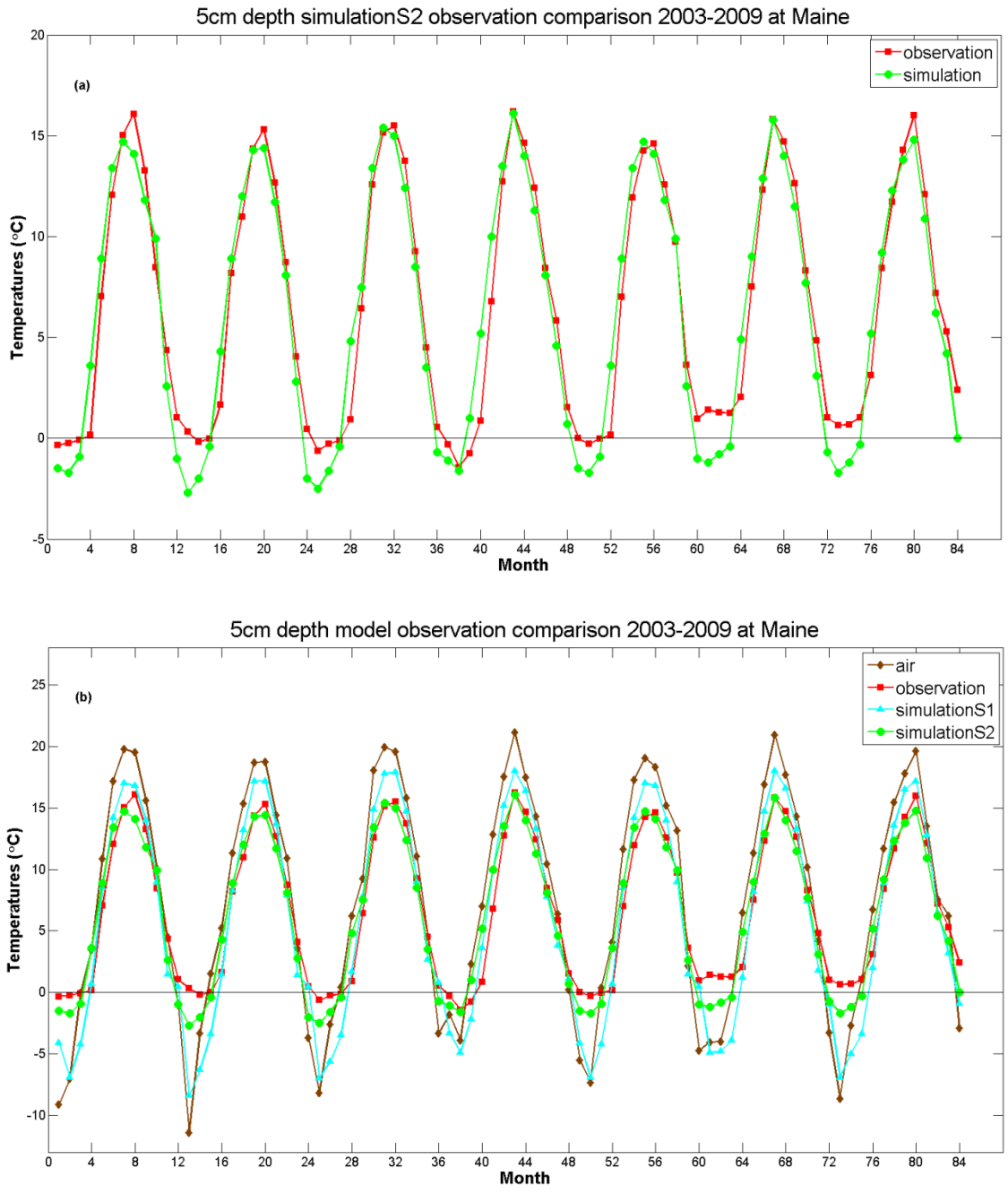

Figure 3-12. (a) Monthly averaged observed and revised simulated soil temperature at 5 cm depth from 2003 to 2009 at the Maine east research site (coniferous forest type). The red line and the squares represent the monthly averaged field-based measurements at 5 cm depth, while the green line and the dots represent the model simulations at the same

depth from revised model. (b) Monthly averaged observations of both air temperature and soil temperature, simulations from the two versions of models at 5 cm depth from 2003 to 2009 at the Maine east research site (coniferous forest type). The red line and the squares represent the monthly averaged field-based measurements at 5 cm depth, the yellow line and the diamonds represent the monthly mean air temperature, the blue line and the triangles represent the original model simulation at 5 cm depth, while the green line and the dots represent the model simulations at the same depth from revised model. The temperatures are displayed in the unit of ℃.

Generally speaking, the simulation results match the field measurements better in warmer months (from May to October in most places) compared to the colder season (from November to the following April). This is understandable in that: (1) the non-frozen soil condition can be better modeled without the need to consider energy loss in phase change and conductivity differences associated with freeze-thaw cycle, and (2) the fact that the snow depth estimation used in the model calculation has unavoidable error from the remotely-sensed snow water equivalent data itself, the spatial variability of snow pack, and the uncertainty of snow pack density, which is not a factor in non-frozen season.

3.2 Regional evaluation results

The calibrated parameters were then used to simulate all model grids. Regional extrapolation results within the spatial domain of 45°N to 72°N continental North America from both models are evaluated using the NARR re-analysis soil temperature estimation at top 10 cm soil depth. Both the NARR estimation and the TEM simulations were averaged into growing season and non-growing season means for the top 10 cm soil temperature, as shown in Figure 3-13, and the differences between the TEM simulations and the NARR estimation are shown in Figure 3-14. The growing season can be very different for different latitudinal zones, and the growing season is from May to October and non-growing season is from November to the next April (Tucker et al., 2001). The eight-year average temperature spatial pattern and the annual time series plot all demonstrate that the revised model performs better (closer to the re-analysis) especially

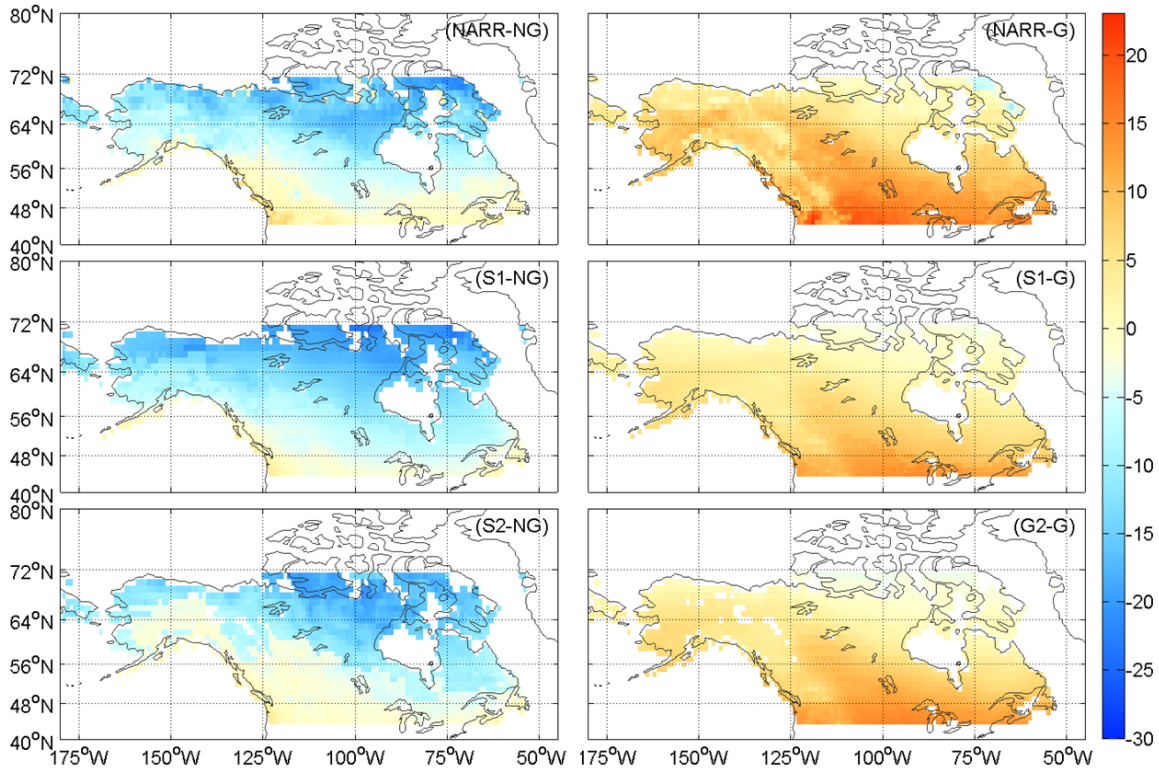

Figure 3-13. Regional evaluation of eight-year averaged non-growing season (left panels) and growing season (right panels) top 10 cm soil temperature comparison between the NARR re-analysis data (NARR), original model (S1), and snow coupled revised model (S2). Temperatures are displayed in the unit of ℃.

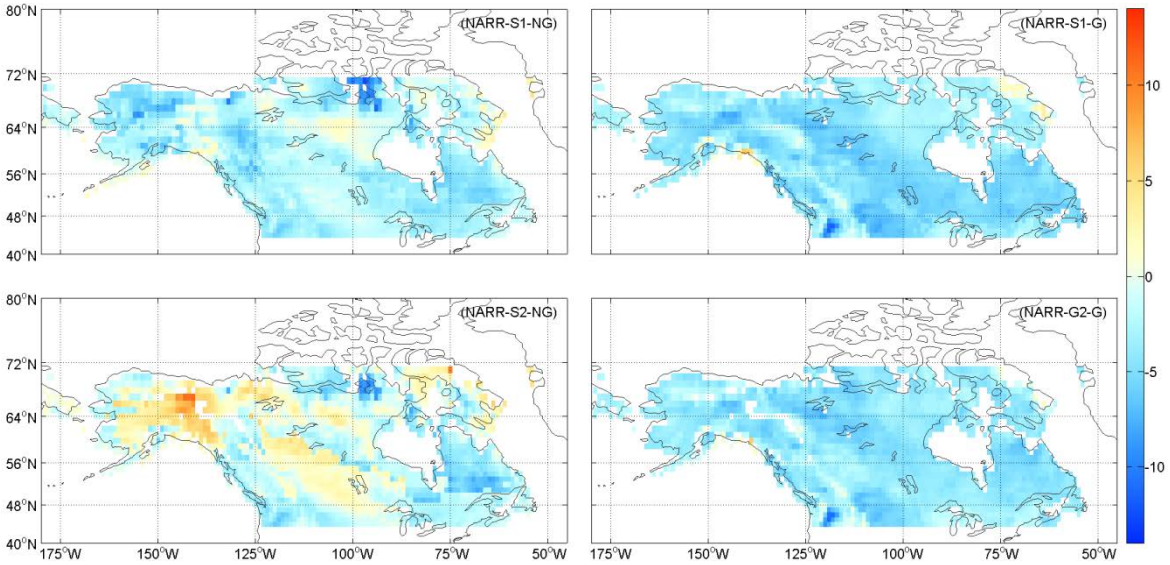

Figure 3-14. Eight-year averaged non-growing season (left panels) and growing season (right panels) regional top 10 cm soil temperature differences between 1) the NARR re-analysis data (NARR) and original model (S1); 2) the NARR re-analysis data (NARR) and snow coupled revised model (S2). Temperatures are displayed in the unit of ℃.

in non-growing season (snow influenced). The non-growing season simulations are around 3℃ warmer using the revised model, yet both models underestimate the growing season topsoil temperature (around $3-4$℃) in comparison with the re-analysis data (Figures 3-13 and 3-15). Apart from the deviant peak in 2006 NARR average, the two simulations all follow the general inter-annual pattern of the NARR dataset (Figure 3-15 and Table 3-2). The reason for the significant deviance in the 2006 re-analysis soil temperature is unknown, given the fact that the 2006 re-analysis data show a much warmer soil temperature (around 4℃) in non-growing season and much colder soil temperature (around 4℃) in growing season compared to other years, while the annual mean air temperature in that year is not significantly different from other years (Figure 2-3). Both the NARR estimation and the TEM simulations show inter-annual variations in the growing and non-growing season top 10 cm soil temperatures, but no noticeable trend is present from 2003 to 2010 according to the spatial average across the region (Figure 3-15). The simulation variations are smaller in magnitude compared to that of the NARR re-analysis data. Overall, considering snow insulation effects improves the estimates of the topsoil temperature over the snow season in northern mid-to-high latitudes.

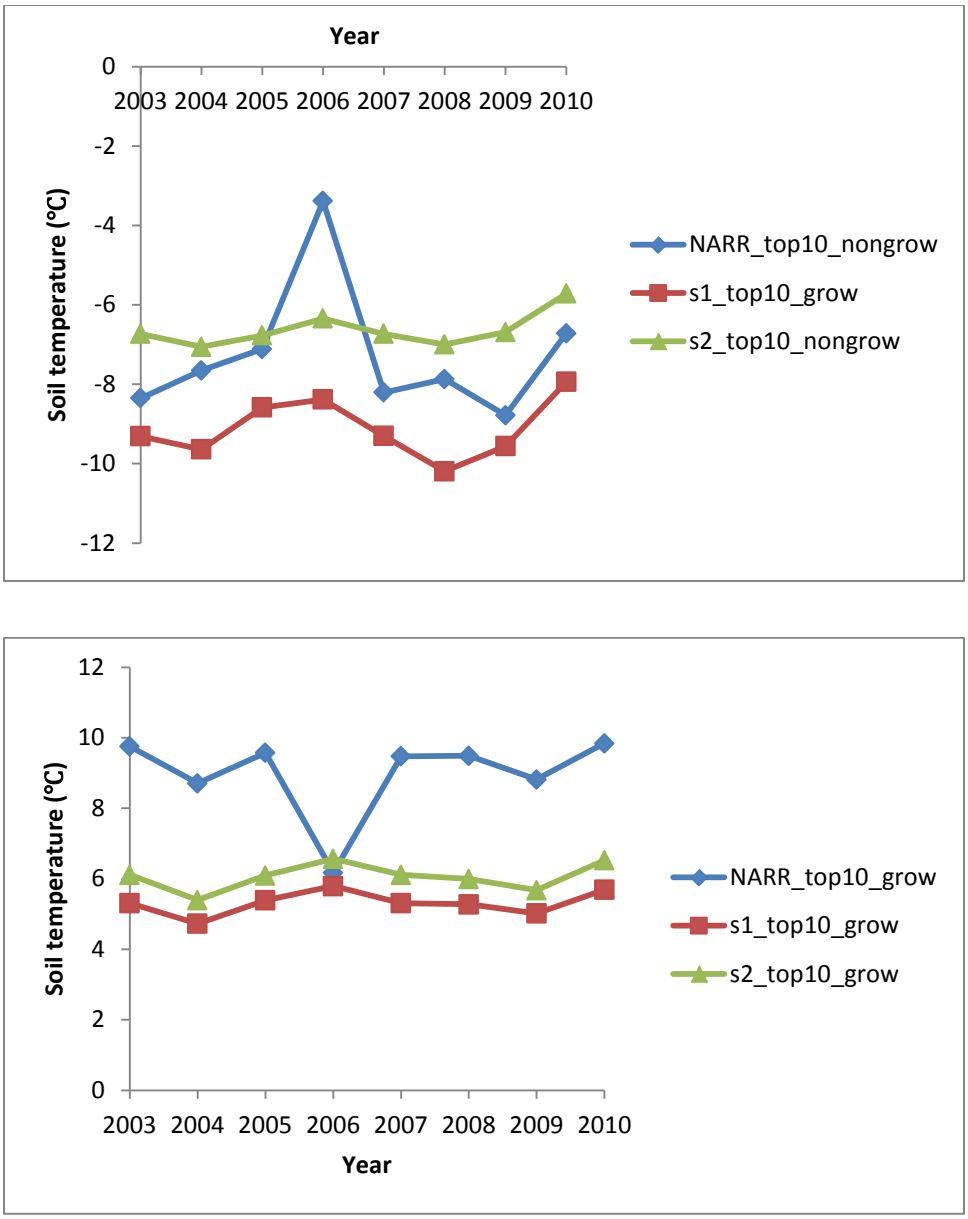

Figure 3-15. Annual non-growing season (upper panel) and growing season (lower panel) top 10 cm soil temperature trend comparison between the NARR re-analysis data (blue line), original model (S1, red line), and snow coupled revised model (S2, green line). Temperatures are displayed in the unit of ℃.

Table 3-2 Regional evaluation of top 10 cm soil temperature using the NARR data for growing and non-growing seasons (℃)

	S1_grow	**S1_nongrow**	**S2_grow**	**S2_nongrow**
RMSE	3.9	2.3	3.2	1.6

3.3 Pan-Arctic simulation results

To better illustrate the prominent effect of snow cover on the soil thermal regime in the region, soil temperature estimates at 5 cm and at 20 cm depths simulated with both models for eight simulation years were mapped (Figures 3-16 to 3-19). The color bars used in these two maps are identical.

Generally speaking, considering the seasonality of the interference from the snow cover, the 5 cm underground soil temperatures of the snow-free summer months (from June to September, (f) - (l) of Figures 3-16.and 3-17) are reasonably close to each other over the entire study area, while in the colder months (from October to the next May, (j) - (e) of Figures 3-16.and 3-17), the soil temperatures have rather large differences between the two versions due to the existence of the snow pack. The rate of soil cooling from October at 5 cm soil layer in the revised soil temperature estimation is lower than that of the original model ((j) of Figures 3-16.and 3-17), and the rate of soil warming in the revised soil temperature estimation from April and May is lower compared with the original model estimation ((d) and (e) of Figures 3-16 and 3-17). The overall mean soil temperatures at 5 cm depth from November to the following March in the revised model estimations are around 5℃ warmer than that of the previous model at the same grid ((c) - (k) of Figures 3-16 and 3-17). This magnitude of increase in soil temperature corresponds well to the observed snow insulation effects on ground thermal from the previous snow manipulation experiment (Hardy et al., 2001). These characteristics are understandable: when there is no snow cover, the two models simulate the soil thermal regime the same,

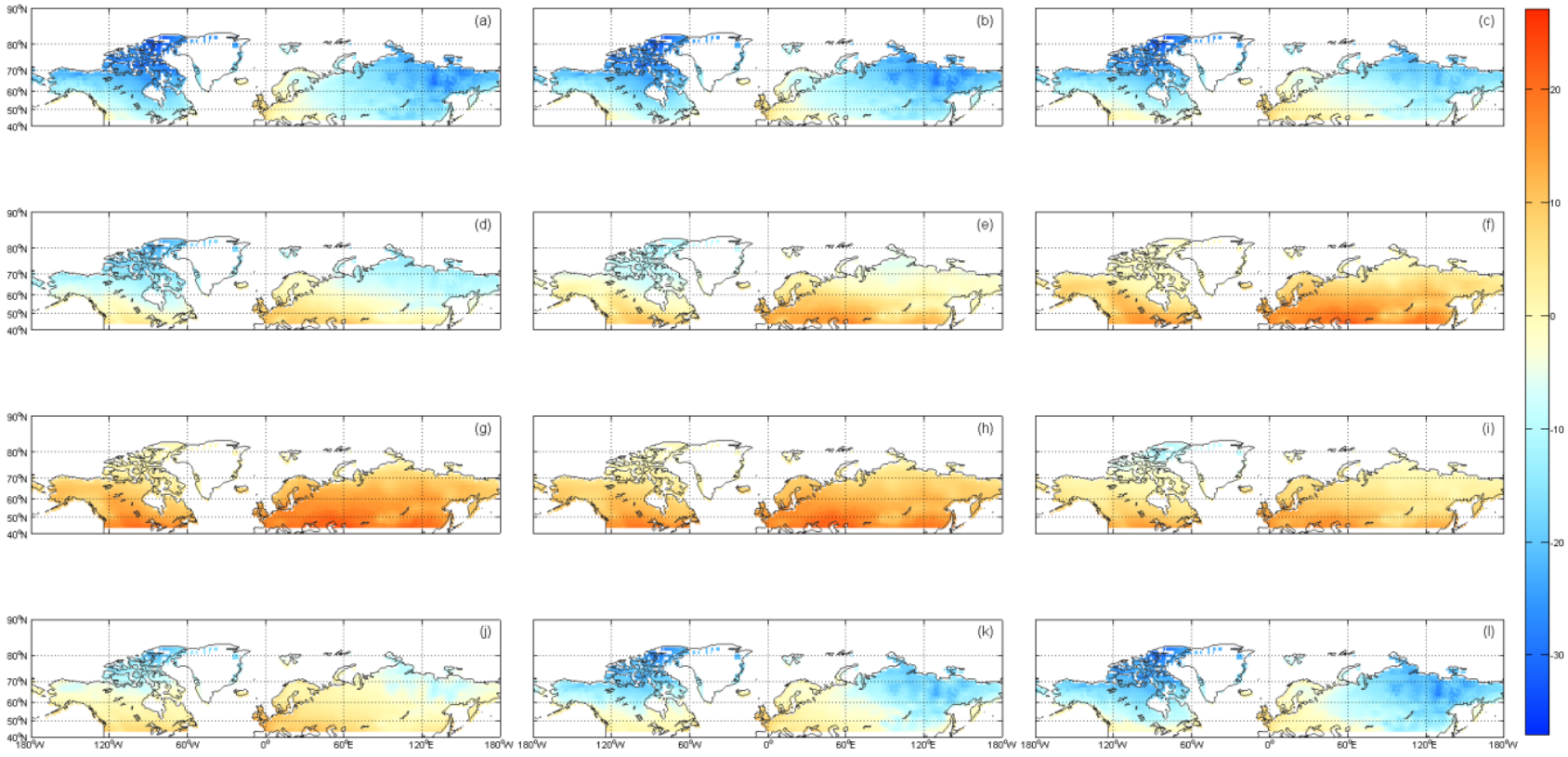

Figure 3-16. Eight-year averaged monthly ((a) – (l)) Pan-arctic regional 5cm underground soil temperature estimates in 2003 obtained from the original STM-TEM model. Temperatures are displayed in the unit of ℃.

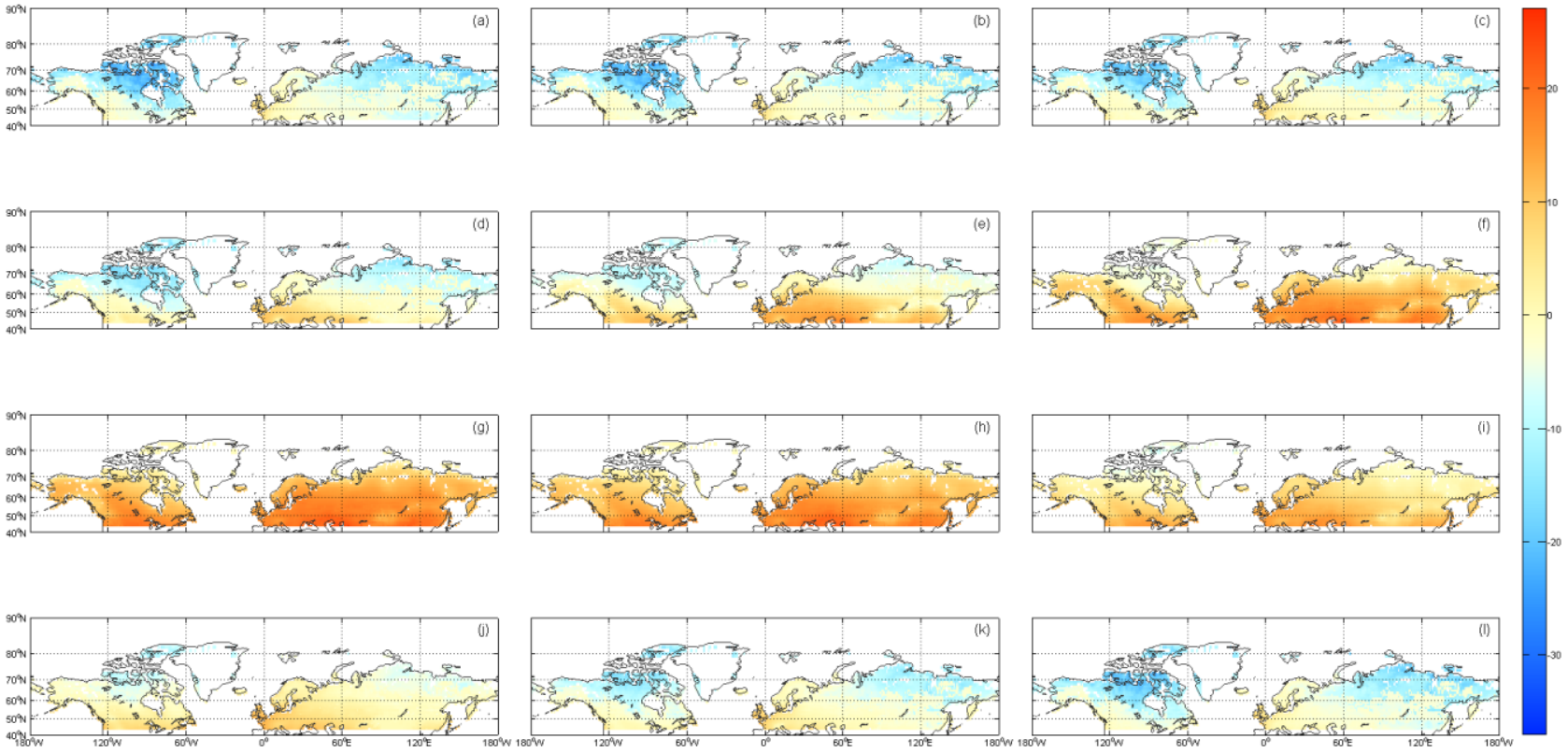

Figure 3-17. Eight-year averaged monthly ((a) – (l)) Pan-arctic regional 5cm underground soil temperature estimates in 2003 obtained from the revised STM-TEM model. Temperatures are displayed in the unit of ℃.

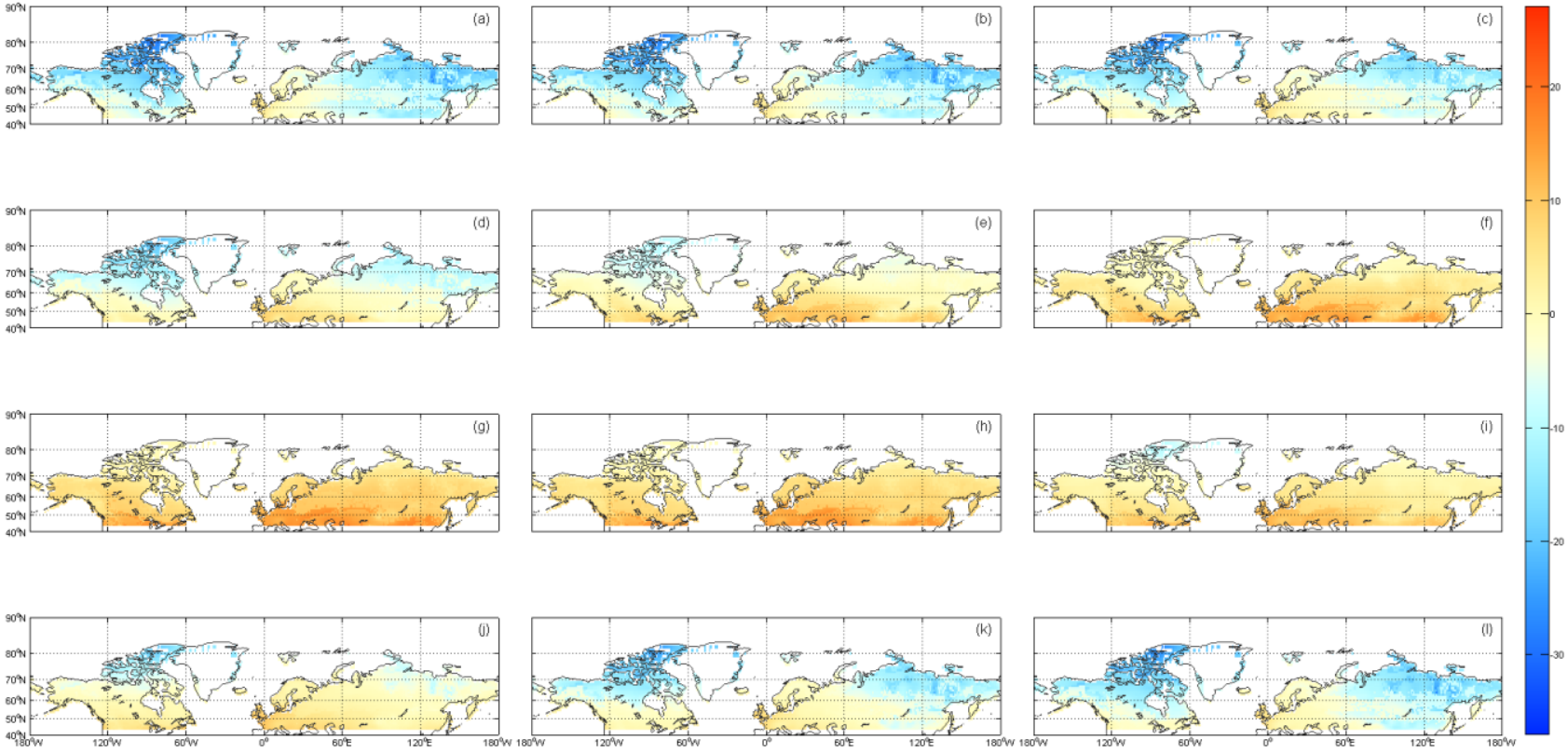

Figure 3-18. Eight-year averaged monthly ((a) – (l)) Pan-arctic regional 20cm underground soil temperature estimates in 2003 obtained from the original STM-TEM model. Temperatures are displayed in the unit of ℃.

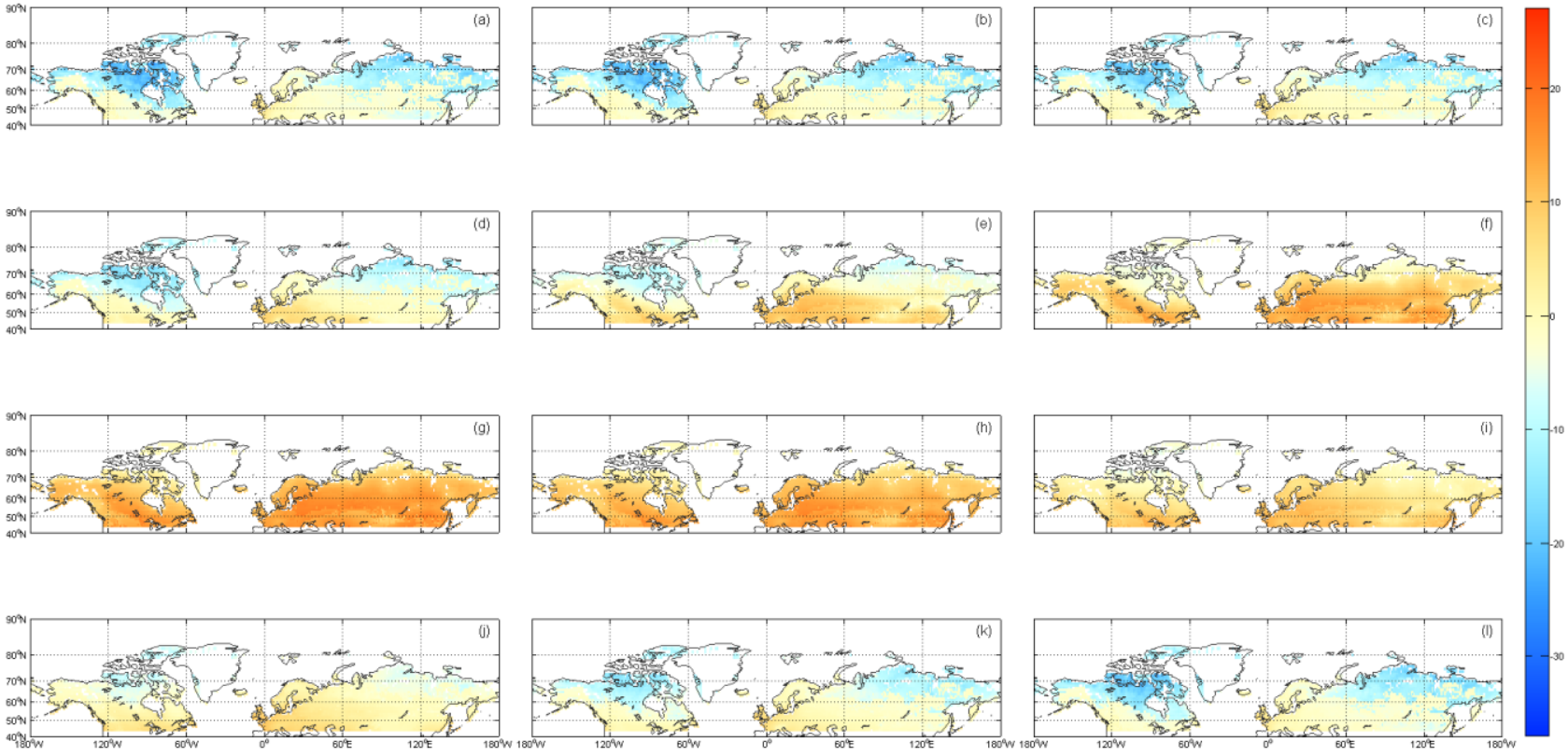

Figure 3-19. Eight-year averaged monthly ((a) – (l)) Pan-arctic regional 20cm underground soil temperature estimates in 2003 obtained from the revised STM-TEM model. Temperatures are displayed in the unit of ℃.

with only soil property values different from the calibration, thus leading to similar soil temperature estimates using the same forcing data. When there is snow cover, the buffering effect of thick snow cover significantly increased the topsoil temperatures from early winter till around April, while the thinner snow layer slightly decreased the topsoil temperatures in the late spring time by impeding soil warming from direct solar radiation. There is an inter-annual variation in the regional soil temperatures, but there is no prominent inter-annual trend, as with the SWE record (Figure 2-6) for the period.

The deeper soil layer at 20 cm depth also exhibits an overall warmer winter (from October to the next May, (j) - (e) of Figures 3-18.and 3-19) soil temperature with the revised model, a delayed soil cooling in the early winter (October, (j) of Figures 3-18.and 3-19) and a delayed soil warming (April to May, (d) and (e) of Figures 3-18.and 3-19) in the late spring. This indicates that there is an insulation effect of snow cover on the soil column as a whole: it increases the temperature of the soil column from top to down, and reduces the frozen depth (defined as the soil layer with temperature lower than $-0.9℃$) of the soil column. The only difference is in the summer time (from June to August, (f) – (h) of Figures 3-18.and 3-19), where the soil temperatures at 20 cm depth simulated with the revised model are slightly higher than that of the original model. The soil temperature difference at 20 cm depth is noticeably smaller, compared with that of at 5 cm depth. This is also confirmed by the snow manipulation experiment at depth from surface to 20 cm to even deeper, the insulation effect of snow on thermal temperatures from top to bottom weakens gradually. This temperature difference with regard to depth is largely due to the difference of the extent of surface snow cover influence on the analyzed soil layer.

The spatial distribution of soil temperature estimates also confirms to the known thermal regime pattern. Soils in southern Alaska are a few degrees warmer than the area in Canada of the same latitude due to the warm current in the Gulf of Alaska, so is the soil temperature in western Europe, which is warmed up by the warm Gulf Stream current. The western Canada including the provinces of Alberta, a large area of British Columbia and the southern part of Saskatchewan which have slightly warmer soils than that of the eastern provinces around the Hudson Bay, which can be attributed to the elevation difference.

The F/T status (whether the ground soil is frozen or not) estimated with the model was assessed and identified based on the near surface soil temperature at 2cm soil depth and the freezing point. The freezing point is practically defined as the highest temperature at which ice can be present in the soil-water system and that the soil can be considered as frozen (Kozlowski, 2004). Pure water freezes theoretically at $0℃$, however, in natural conditions, water does not start to freeze at $0℃$, rather, a supercooling temperature lower than $0℃$ needs to be reached. For a similar reason, and considering the existence of minerals in the soil-water system, the freezing point of ground soil should be lower than $0℃$. Scientists have conducted many experiments using different types of soils to examine their actual freezing points (Kozlowski, 2004; Rivkina et al., 2000; Kozlowski, 2009). Here an average $-0.9℃$ obtained from the empirical sample test and equation given in literatures (Rivkina et al., 2000; Kozlowski, 2009) is used as the freezing point to classify the ground F/T status. Grid cells with soil temperatures below $-0.9℃$ were defined as frozen, above or equal to $-0.9℃$ as non-frozen.

Because almost all the near surface soil in the study area is actually frozen in winter (from December to the following March) and almost all of the near surface soil is thawed in summer (from June to September), F/T status from May and November for each year were selected to compare, due to the fact that the results from these two months are more different. Differences between the F/T status of the two model simulations is weakened in comparison to that of the soil temperatures due to the fact that the values are binary in value, but can still be noted. The frozen/non-frozen dividing line ($-0.9℃$ isotherm line as in this case) moves a bit southward in the late spring time (May) in the revised model compared to the original model, corresponding to the slower soil warming discussed previously (Figure 3-20); and moves slightly northward in the early winter (November) in the revised model than in the original model (Figure 3-21), due to the insulation effect of snow on soil column. For the same reason, the annual May frozen and non-frozen area percentages of the revised model are closer to the observation, in comparison with those of the original model (Figures 3-22 and 3-23). The comparison between the annual May and November frozen and non-frozen area percentage plots indicates that model estimates are closer to each other in November than in May (Figures 3-22 and 3-23). This is largely attributed to the fact that the estimated soil thermal regimes are close in the early winter given the limited influence of snow and similar summer-fall soil temperatures. Overall, the revised model performs better, and the difference between the two simulations is noticeably larger in May due to accumulated snow influence on the soil column in winter.

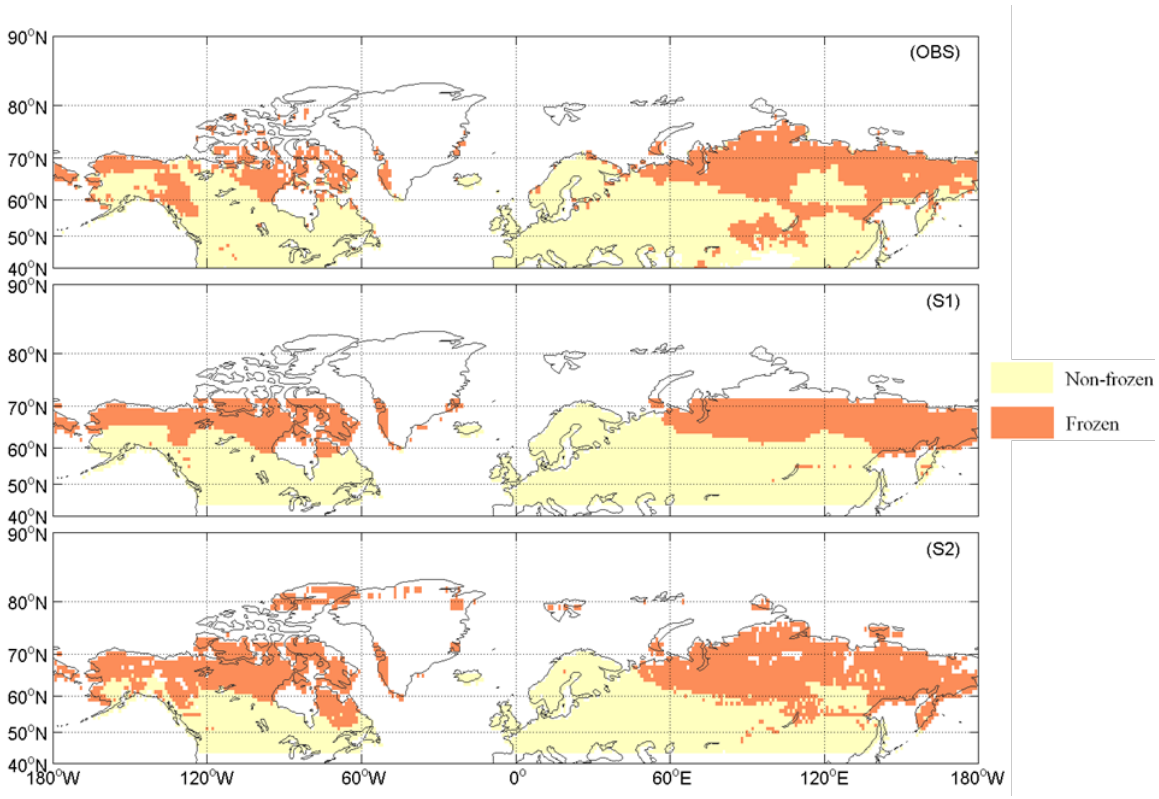

Figure 3-20. Freeze/thaw status in May, 2006 over the study area from (1) monthly averaged MEaSUREs Freeze/Thaw Status (OBS), (2) monthly averaged freeze/thaw status simulation from the original model (S1), and (3) monthly averaged freeze/thaw status simulation from the revised model (S2).

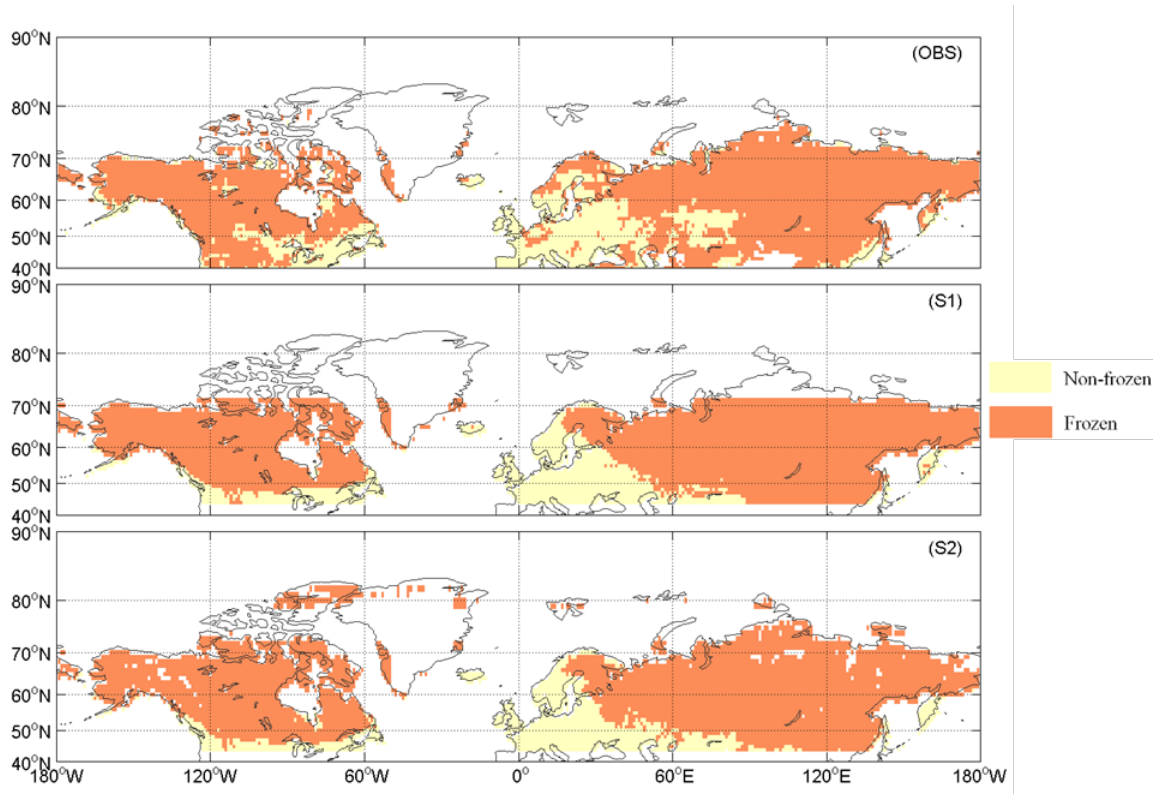

Figure 3-21. Freeze/thaw status in November, 2006 over the study area from (1) monthly averaged MEaSUREs Freeze/Thaw Status (OBS), (2) monthly averaged freeze/thaw status simulation from the original model (S1), and (3) monthly averaged freeze/thaw status simulation from the revised model (S2).

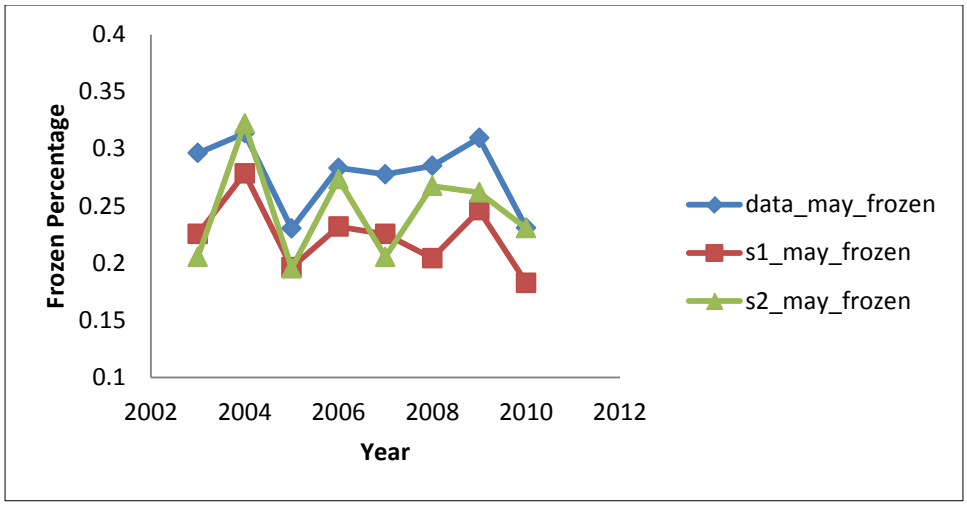

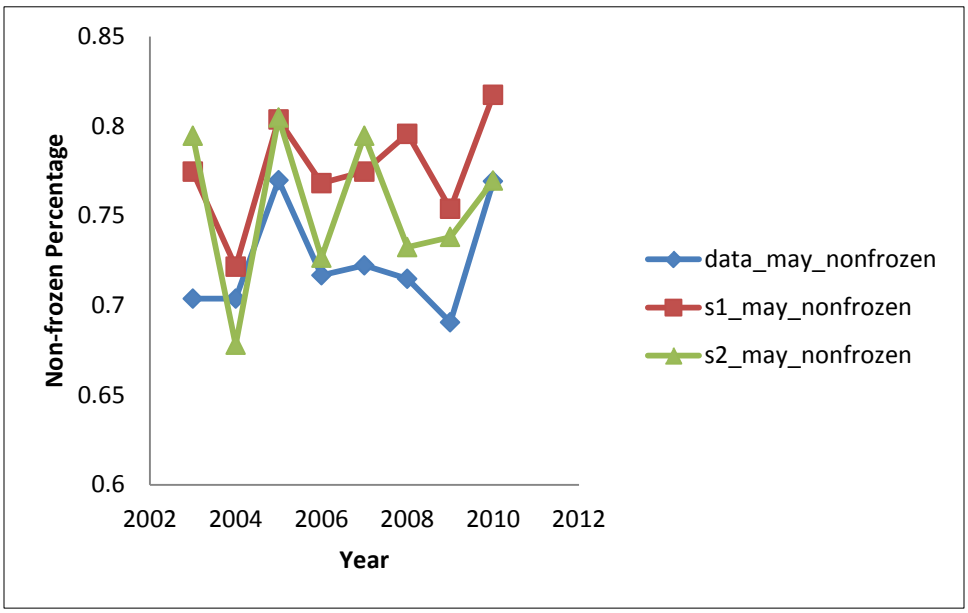

Figure 3-22. Annual frozen and non-frozen area percentage comparison for surface soil in May between the satellite observation (blue line), the original model simulation (S1, red line), and the snow revised model simulation (S2, green line) from 2003 to 2010.

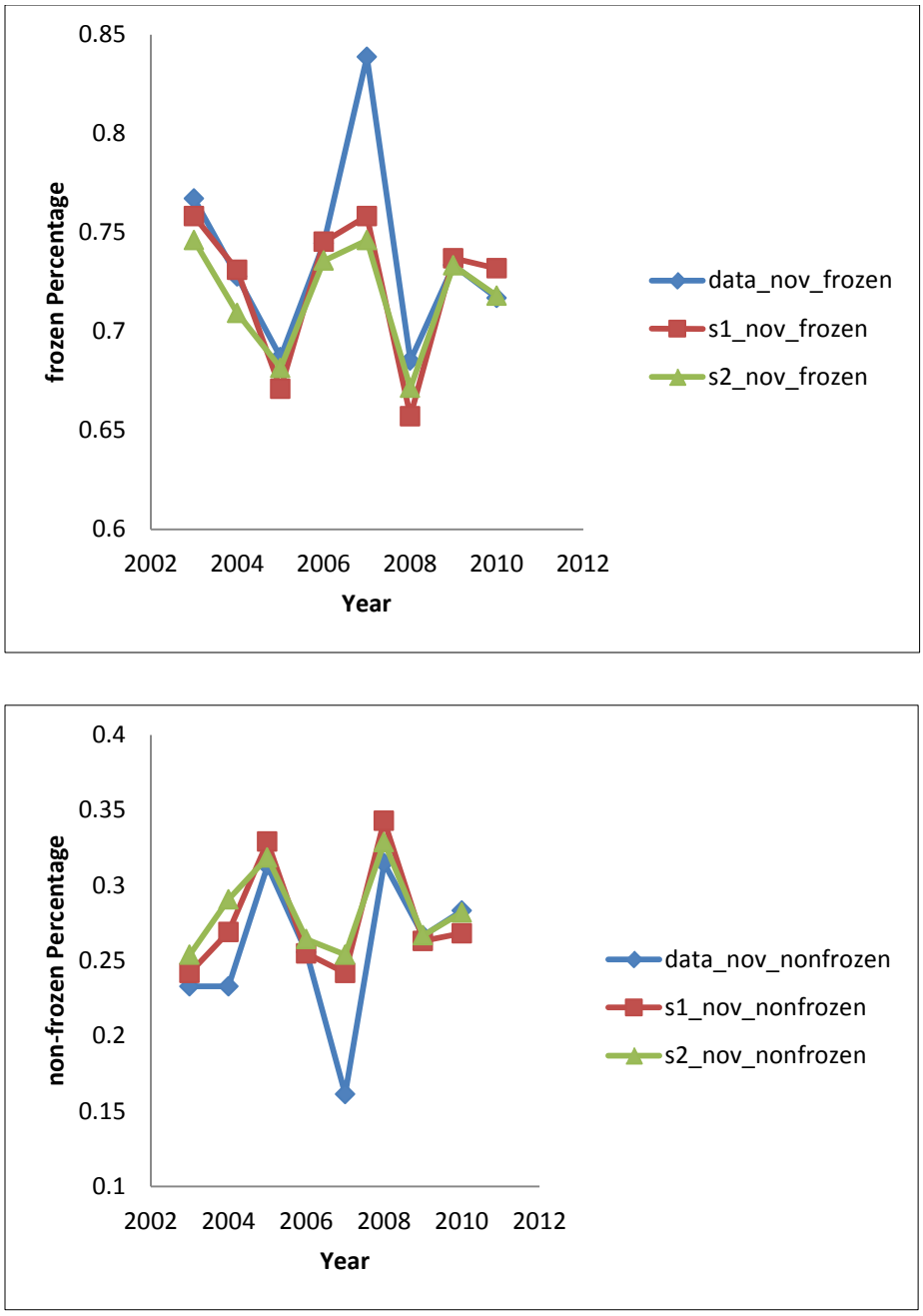

Figure 3-23. Annual frozen and non-frozen area percentage comparison for surface soil in November between the satellite observation (blue line), the original model simulation (S1, red line), and snow revised model simulation (S2, green line) from 2003 to 2010.

CHAPTER 4. CONCLUSIONS

In this study, the snow insulation effect in the revised TEM was calibrated for northern higher latitudes using in situ climate and soil thermal observation data. The calibration and evaluation showed that the revised model performs better in estimating the topsoil temperature profiles that are closer to observations for each calibration site in the region. The calibrated model was then used to simulate the soil thermal regime across the area north of 45°N from year 2003 to year 2010. In addition to the climate, soil texture, elevation, and vegetation data that are used to drive the original model, satellite snow water equivalent data are used to drive the revised model in estimating snow insulation effects. The simulated seasonal average topsoil layer temperature profiles, freeze/thaw status, and freeze/thaw area percentage from the two versions of models are analyzed. Insulation effects of snow affect soil thermal regime at 5cm and 20cm depth, respectively. The revised model estimates a temperature increase of more than 5℃ in winter compared to that of the original model, as well as a delay of soil cooling in early winter and a lag of soil warming in late spring. The presence of snow influences ground freeze/thaw status. The frozen front estimated by the revised model moves slightly southward in late spring and slightly northward in early winter. This study suggests the prominence role of snow cover on northern ecosystems, which deserves further studies using more observational data of snow in recent decades.

CHAPTER 5. LIMITATION AND FUTURE WORK

In this study, the coupled STM-TEM modeling system is calibrated and satellite derived snow depth data is used to improve soil thermal regime simulation. However, there are a number of limitations to this study. First, the revised modeling system was calibrated to a limited number of sets of observation data for a limited number of vegetation and soil types. The calibration datasets were all obtained from North America and are of relatively short temporal extent in most cases. Moreover, these datasets include only the soil thermal regime records of the topsoil layers. With more data becoming available, such as the new field observation sites added to the AmeriFlux system, a more comprehensive study that utilizes various site-level climate and soil thermal records for all vegetation and soil types would eventually contribute to a more generally acceptable modeling system that would yield more robust and acceptable conclusions. In fact, there have been more international collaborations in sharing soil related observation records across the northern higher latitudes (http://gtnpdatabase.org/). Borehole soil temperature and soil moisture to deep depths (even over a hundred meters deep) measured in Russia, Sweden, Switzerland, Austria and Italy in addition to North America sites are now available for more a comprehensive study (Boike et al., 2013). Second, because site-level snow depth or snow water equivalent data is not available, all sites are calibrated using AMSR-E satellite SWE as described in the previous section. The spatial variability of

snow pack due to topography, vegetation cover and blowing wind adds to simulation error when applied to site-level modeling. In order to solve the inhomogeneity influence of snow input on soil thermal simulation with a lack of field based snow pack observations, a dynamic process-based snow model is needed, which will be part of my future work. Third, soil moisture and soil temperature are related, yet we did not include a feedback of soil moisture to soil temperature. This interaction between the soil temperature and soil moisture would affect soil thermal dynamics. Fourth, parameter sensitivity analysis is not included in this thesis, which will be helpful in understanding the simulation uncertainty due to model structure.

My future work will focus on: first, replacing the input satellite snow depth information with model simulated snow depth. Major snow accumulation dynamics include snow melting, refreezing, outflow and sublimation processes will be explicitly modeled, instead of directly using snow depth data from observations. The current STM-TEM simply estimates snow from precipitation based on air temperature. In a planned new snow modeling scheme, the initial snow amount will be altered daily. Snow melting and refreezing processes are directly related to air temperature, and are regulated by degree-day factor. The snow pack itself can hold certain amount of liquid water, which is dependent on its retention capacity. Sublimation occurs when the temperature and pressure are extremely low, changing solid snow directly into the gas phase. This can be estimated using solar radiation incident on the snow surface and latent heat that would occur in the process. These processes have been analyzed and can be modeled preferably on a daily basis (e.g., Karvonen, 2003; Tang and Zhuang, 2011). With the available satellite-based snow water equivalent data for evaluation, I can simulate snow dynamics

explicitly. After I successfully model the soil thermal dynamics, I will model the changes of microbial activities and their effects on soil carbon dynamics in response to the changing soil thermal regime induced by the insulation of snow cover. Modifications in soil freeze/thaw conditions and thermal profile can lead to shifts in the growing season, soil respiration and gross primary productivity, thus altering carbon cycle in the northern high latitudes. Previous research using CNDM (carbon/nitrogen dynamics module) coupled with TEM model have been conducted on the Tibetan Plateau (Jin et al., 2015; Zhuang, Q., et al., 2010), demonstrating reasonably good performance in estimating carbon fluxes and pool sizes of terrestrial ecosystems. I will further develop this coupled system to examine how snow would affect the carbon dioxide and methane exchanges between the ecosystems and the atmosphere. Thirdly, I plan to model the snow photolysis chemistry based on a snow pack model. Observations have confirmed that the snow pack acts as a complex multiphase photochemical reactor that is actively involved in modifying the chemical composition, including ozone, nitrogen oxides, BrO and OH radical, of the atmosphere above (Dominé and Shepson, 2002; Domine et al., 2008). Quantifying these chemical emissions from the sunlit snow pack is important to modeling global nitrogen cycling and the atmospheric boundary layer process. Physical and chemical models such as MISTRA-SNOW model have been developed to examine snow-to-atmosphere fluxes of NO_2 due to the photolysis of the absorbed NO_3^- in the atmosphere-snow boundary layer over the Greenland ice sheets (Thomas et al., 2011; Glasow et al., 2002a, b). Incorporating my explicit snow model into these snow chemical models shall improve the snow chemistry modeling in the region.

REFERENCES

REFERENCES

Amiro, B. D., et al. "Carbon, energy and water fluxes at mature and disturbed forest sites, Saskatchewan, Canada." Agricultural and forest meteorology 136.3 (2006): 237-251.

Beniston, Martin. "Variations of snow depth and duration in the Swiss Alps over the last 50 years: links to changes in large-scale climatic forcings." Climatic Change 36.3-4 (1997): 281-300.

Boike, J., et al. "Baseline characteristics of climate, permafrost and land cover from a new permafrost observatory in the Lena River Delta, Siberia (1998-2011)." Biogeosciences 10.3 (2013): 2105-2128.

Brown, Ross D., Bruce Brasnett, and David Robinson. "Gridded North American monthly snow depth and snow water equivalent for GCM evaluation." Atmosphere-Ocean 41.1 (2003): 1-14.

Brown, R. D., and D. A. Robinson. "Northern Hemisphere spring snow cover variability and change over 1922–2010 including an assessment of uncertainty." The Cryosphere 5.1 (2011): 219-229.

Brown, Ross D., and Philip W. Mote. "The response of northern hemisphere snow cover to a changing climate*." Journal of Climate 22.8 (2009): 2124-2145.

Cherkauer, Keith A., and Dennis P. Lettenmaier. "Hydrologic effects of frozen soils in the upper Mississippi River basin." Journal of Geophysical Research: Atmospheres (1984–2012) 104.D16 (1999): 19599-19610.

Déry, Stephen J., and Ross D. Brown. "Recent Northern Hemisphere snow cover extent trends and implications for the snow‐albedo feedback." Geophysical Research Letters 34.22 (2007). "An observation-based assessment of the influences of air temperature and snow depth on soil temperature in Russia." Environmental Research Letters 9.6 (2014): 064026.

Desai, Ankur R., et al. "Comparing net ecosystem exchange of carbon dioxide between an old-growth and mature forest in the upper Midwest, USA." Agricultural and Forest Meteorology 128.1 (2005): 33-55.

Dominé, Florent, and Paul B. Shepson. "Air-snow interactions and atmospheric chemistry." Science 297.5586 (2002): 1506-1510.

Domine, F., et al. "Snow physics as relevant to snow photochemistry." Atmospheric chemistry and physics 8.2 (2008): 171-208.

Dugua, Claude R., and Alain Pietroniro. Remote sensing in northern hydrology: measuring environmental change. Vol. 163. American Geophysical Union, 2005.

Dyer, Jamie L., and Thomas L. Mote. "Spatial variability and trends in observed snow depth over North America." Geophysical Research Letters 33.16 (2006).

Edenhofer, O., et al. "IPCC, 2014: Climate Change 2014: Mitigation of Climate Change. Contribution of Working Group III to the Fifth Assessment Report of the Intergovernmental Panel on Climate Change." Transport (2014).

Ek M B, Mitchell K E, Lin Y, et al. Implementation of Noah land surface model advances in the National Centers for Environmental Prediction operational mesoscale Eta model[J]. Journal of Geophysical Research: Atmospheres (1984–2012), 2003, 108(D22).

Euskirchen, E. S., et al. "Importance of recent shifts in soil thermal dynamics on growing season length, productivity, and carbon sequestration in terrestrial high‐latitude ecosystems." Global Change Biology 12.4 (2006): 731-750.

Felzer, B., et al. "Future effects of ozone on carbon sequestration and climate change policy using a global biogeochemical model." Climatic Change 73.3 (2005): 345-373.

Gaige, E., et al. "Changes in canopy processes following whole-forest canopy nitrogen fertilization of a mature spruce-hemlock forest." Ecosystems 10.7 (2007): 1133-1147.

Goodrich, Laurel Everett. A numerical model for assessing the influence of snow cover on the ground thermal regime. 1976.

Gorham, Eville. "Northern peatlands: role in the carbon cycle and probable responses to climatic warming." Ecological applications 1.2 (1991): 182-195.

Hardy, Janet P., et al. "Snow depth manipulation and its influence on soil frost and water dynamics in a northern hardwood forest." Biogeochemistry 56.2 (2001): 151-174.

Ikawa, Hiroki, and Walter C. Oechel. "Spatial and temporal variability of air-sea CO 2 exchange of alongshore waters in summer near Barrow, Alaska." Estuarine, Coastal and Shelf Science 141 (2014): 37-46.

Iman, Ronald L. "Latin hypercube sampling." Encyclopedia of quantitative risk analysis and assessment (2008).

Jin, Zhenong, et al. "Net exchanges of methane and carbon dioxide on the Qinghai-Tibetan Plateau from 1979 to 2100." Environmental Research Letters 10.8 (2015): 085007.

Karvonen, T. "Influence of global climatic change on different hydrological variables." (2003).

Kozlowski, Tomasz. "Soil freezing point as obtained on melting." Cold Regions Science and Technology 38.2 (2004): 93-101.

Kozlowski, Tomasz. "Some factors affecting supercooling and the equilibrium freezing point in soil–water systems." Cold Regions Science and Technology 59.1 (2009): 25-33.

Lawrence, David M., and Andrew G. Slater. "The contribution of snow condition trends to future ground climate." Climate Dynamics 34.7-8 (2010): 969-981.

Lemke, Peter, et al. "Observations: changes in snow, ice and frozen ground." (2007).

McCarthy, James J. Climate change 2001: impacts, adaptation, and vulnerability: contribution of Working Group II to the third assessment report of the Intergovernmental Panel on Climate Change. Cambridge University Press, 2001.

McCaughey, J. Harry, et al. "Magnitudes and seasonal patterns of energy, water, and carbon exchanges at a boreal young jack pine forest in the BOREAS northern study area." Journal of Geophysical Research: Atmospheres (1984–2012) 102.D24 (1997): 28997-29007.

McGuire, A. David, et al. "Interactions between carbon and nitrogen dynamics in estimating net primary productivity for potential vegetation in North America." Global Biogeochemical Cycles 6.2 (1992): 101-124.

McGuire, A. David, et al. "Equilibrium responses of soil carbon to climate change: empirical and process-based estimates." Journal of Biogeography (1995): 785-796.

McGuire, A. David, Jerry M. Melillo, and Linda A. Joyce. "The role of nitrogen in the response of forest net primary production to elevated atmospheric carbon dioxide." Annual Review of Ecology and systematics (1995): 473-503.

McGuire, A. David, et al. "Equilibrium responses of global net primary production and carbon storage to doubled atmospheric carbon dioxide: Sensitivity to changes in vegetation nitrogen concentration." Global Biogeochemical Cycles 11.2 (1997): 173-189.

Mesinger F, DiMego G, Kalnay E, et al. North American regional reanalysis[J]. Bulletin of the American Meteorological Society, 2006, 87(3): 343-360.

Mitchell, Timothy D., et al. "A comprehensive set of high-resolution grids of monthly climate for Europe and the globe: the observed record (1901–2000) and 16 scenarios (2001–2100)." Tyndall Centre for Climate Change Research Working Paper 55.0 (2004): 25.

Osterkamp, T. E., and J. P. Gosink. "Variations in permafrost thickness in response to changes in paleoclimate." Journal of Geophysical Research: Solid Earth (1978–2012) 96.B3 (1991): 4423-4434.

Osterkamp, T. E., and V. E. Romanovsky. "Evidence for warming and thawing of discontinuous permafrost in Alaska." Permafrost and Periglacial Processes 10.1 (1999): 17-37.

Osterkamp, T. E. "Characteristics of the recent warming of permafrost in Alaska." Journal of Geophysical Research: Earth Surface (2003–2012) 112.F2 (2007).

Park, Hotaek, et al. "An observation-based assessment of the influences of air temperature and snow depth on soil temperature in Russia." Environmental Research Letters 9.6 (2014): 064026.

Raich, J. W., et al. "Potential net primary productivity in South America: application of a global model." Ecological Applications 1.4 (1991): 399-429.

Rivkina, E. M., et al. "Metabolic activity of permafrost bacteria below the freezing point." Applied and Environmental Microbiology 66.8 (2000): 3230-3233.

Serreze, Mark C., and Jennifer A. Francis. "The Arctic amplification debate." Climatic Change 76.3-4 (2006): 241-264.

Stieglitz, Marc, et al. "The role of snow cover in the warming of arctic permafrost." Geophysical Research Letters 30.13 (2003).

Sturm, Matthew, Jon Holmgren, and Glen E. Liston. "A seasonal snow cover classification system for local to global applications." Journal of Climate 8.5 (1995): 1261-1283.

Sturm, Matthew, et al. "The thermal conductivity of seasonal snow." Journal of Glaciology 43.143 (1997): 26-41.

Sturm, Matthew, et al. "Snow-shrub interactions in Arctic tundra: a hypothesis with climatic implications." Journal of Climate 14.3 (2001): 336-344.

Sturm, Matthew, et al. "Estimating snow water equivalent using snow depth data and climate classes." Journal of Hydrometeorology 11.6 (2010): 1380-1394.

Tang, Jinyun, and Qianlai Zhuang. "Modeling soil thermal and hydrological dynamics and changes of growing season in Alaskan terrestrial ecosystems." Climatic change 107.3-4 (2011): 481-510.

Tarnocai, Charles, et al. "Soil organic carbon pools in the northern circumpolar permafrost region." Global biogeochemical cycles 23.2 (2009).

Thomas, Jennie L., et al. "Modeling chemistry in and above snow at Summit, Greenland–Part 1: Model description and results." Atmospheric Chemistry and Physics 11.10 (2011): 4899-4914.

Tucker, Compton J., et al. "Higher northern latitude normalized difference vegetation index and growing season trends from 1982 to 1999." International journal of biometeorology 45.4 (2001): 184-190.

Ueyama, Masahito, et al. "Growing season and spatial variations of carbon fluxes of Arctic and boreal ecosystems in Alaska (USA)." Ecological Applications 23.8 (2013): 1798-1816.

von Glasow, Roland, et al. "Modeling halogen chemistry in the marine boundary layer 1. Cloud‐free MBL." Journal of Geophysical Research: Atmospheres (1984–2012) 107.D17 (2002): ACH-9.

von Glasow, Roland, et al. "Modeling halogen chemistry in the marine boundary layer 2. Interactions with sulfur and the cloud‐covered MBL." Journal of Geophysical Research: Atmospheres (1984–2012) 107.D17 (2002): ACH-2.

Vorosmarty, C. J., and A. L. Schloss. "Global climate change and terrestrial net primary production." Nature 363.234240 (1993): 359378.

Yi, Y., et al. "The role of snow cover and soil freeze/thaw cycles affecting boreal-arctic soil carbon dynamics." Biogeosciences Discussions 12.14 (2015).

Zhang, Yinsuo, et al. "Impact of snow cover on soil temperature and its simulation in a boreal aspen forest." Cold Regions Science and Technology 52.3 (2008): 355-370.

Zhuang, Q., V. E. Romanovsky, and A. D. McGuire. "Incorporation of a permafrost model into a large‐scale ecosystem model: Evaluation of temporal and spatial scaling issues in simulating soil thermal dynamics." Journal of Geophysical Research: Atmospheres (1984–2012) 106.D24 (2001): 33649-33670.

Zhuang, Q., et al. "Modeling soil thermal and carbon dynamics of a fire chronosequence in interior Alaska." Journal of Geophysical Research: Atmospheres (1984–2012) 107.D1 (2002): FFR-3.

Zhuang, Q., et al. "Carbon cycling in extratropical terrestrial ecosystems of the Northern Hemisphere during the 20th century: a modeling analysis of the influences of soil thermal dynamics." Tellus B 55.3 (2003): 751-776.

Zhuang, Q., et al. "Methane fluxes between terrestrial ecosystems and the atmosphere at northern high latitudes during the past century: A retrospective analysis with a process‐based biogeochemistry model." Global Biogeochemical Cycles 18.3 (2004).

Zhuang, Q., et al. "Carbon dynamics of terrestrial ecosystems on the Tibetan Plateau during the 20th century: an analysis with a process‐based biogeochemical model." Global Ecology and Biogeography 19.5 (2010): 649-662.